Late Paleozoic Chingiz and Saur Arc Amalgamation in West Junggar (NW China): Implications for Accretionary Tectonics in the Southern Altaids

Shuaihua Song, Wenjiao Xiao, Brian F. Windley, A. S. Collins, Yichao Chen, Ji'En Zhang, Karel Schulmann, Chunming Han, Bo Wan, Songjian Ao, et al.

▶ **To cite this version:**

Shuaihua Song, Wenjiao Xiao, Brian F. Windley, A. S. Collins, Yichao Chen, et al.. Late Paleozoic Chingiz and Saur Arc Amalgamation in West Junggar (NW China): Implications for Accretionary Tectonics in the Southern Altaids. Tectonics, 2020, 39, ⟨10.1029/2019TC005781⟩. ⟨insu-03707757⟩

HAL Id: insu-03707757

https://insu.hal.science/insu-03707757v1

Submitted on 1 Jul 2022

HAL is a multi-disciplinary open access archive for the deposit and dissemination of scientific research documents, whether they are published or not. The documents may come from teaching and research institutions in France or abroad, or from public or private research centers.

L'archive ouverte pluridisciplinaire **HAL**, est destinée au dépôt et à la diffusion de documents scientifiques de niveau recherche, publiés ou non, émanant des établissements d'enseignement et de recherche français ou étrangers, des laboratoires publics ou privés.

Copyright - All rights reserved

Check for updates

AGU ADVANCING EARTH AND SPACE SCIENCE

Tectonics

RESEARCH ARTICLE
10.1029/2019TC005781

Key Points:
- The Hebukesaier mélange contains ocean crust blocks generated in an N-MORB setting in the late Cambrian and late Carboniferous
- The Chingiz Arc and subduction complex was generated by southward subduction of the Paleo-Asian Ocean, which closed before the late Triassic
- The Saur and Chingiz arcs were merged by opposite subduction; the mélange occupies the boundary separating the Chingiz Arc from the Saur Arc

Supporting Information:
- Supporting Information S1

Correspondence to:
W. Xiao,
wj-xiao@mail.iggcas.ac.cn

Citation:
Song, S., Xiao, W., Windley, B. F., Collins, A. S., Chen, Y., Zhang, J., et al. (2020). Late Paleozoic Chingiz and Saur Arc Amalgamation in West Junggar (NW China): Implications for Accretionary Tectonics in the Southern Altaids. *Tectonics*, *39*, e2019TC005781. https://doi.org/10.1029/2019TC005781

Received 21 JUL 2019
Accepted 31 MAY 2020
Accepted article online 2 JUN 2020

©2020. American Geophysical Union. All Rights Reserved.

Late Paleozoic Chingiz and Saur Arc Amalgamation in West Junggar (NW China): Implications for Accretionary Tectonics in the Southern Altaids

Shuaihua Song[1,3,4], Wenjiao Xiao[1,2,3], Brian F. Windley[5], A. S. Collins[6], Yichao Chen[3], Ji'en Zhang[1,4], Karel Schulmann[7,8], Chunming Han[1,4], Bo Wan[1,4], Songjian Ao[1,4], Zhiyong Zhang[1,4], Dongfang Song[1,4], and Rui Li[1,3,4]

[1]State Key Laboratory of Lithospheric Evolution, Institute of Geology and Geophysics, Chinese Academy of Sciences, Beijing, China, [2]Xinjiang Research Center for Mineral Resources, Xinjiang Institute of Ecology and Geography, Chinese Academy of Sciences, Urumqi, China, [3]College of Earth and Planetary Sciences, University of Chinese Academy of Sciences, Beijing, China, [4]Innovation Academy for Earth Sciences, Chinese Academy of Sciences, Beijing, China, [5]Department of Geology, The University of Leicester, Leicester, UK, [6]Tectonics and Earth Systems Group, Department of Earth Sciences, The University of Adelaide, Adelaide, SA, Australia, [7]Institut de Physique du Globe de Strasbourg, MMR7516, University of Strasbourg/EOST, CNRS, Strasbourg, France, [8]Department of Lithospheric Research, Czech Geological Survey, Praha 1, Czech Republic

Abstract The Saur-Chingiz Belt (SCB) in northern West Junggar is regarded as the amalgamation zone of the Saur and Chingiz arcs. It contains diagnostic rocks of accretionary origin, providing critical information about the evolution of the southern Paleo-Asian Ocean. We recognize various lithologies in the SCB, including an ophiolitic mélange, turbidites, conglomerates, rhyolites, breccias, and diorites, and investigate the structures of the Hebukesaier ophiolitic mélange. Kinematic analysis indicates top-to-the-N thrusting. A coarse-grained gabbro (ca. 490 Ma) and a fine-grained gabbro (ca. 318 Ma) have normal mid-ocean ridge basalt (N-MORB)-type geochemical signatures, and three groups of pillow basalts exhibit N-MORB, enriched mid-ocean ridge basalt (E-MORB), and ocean island basalts (OIB) fingerprints, respectively. Detrital zircons in tuffs, conglomerates, and turbidites associated with the Hebukesaier mélange display predominant ages of 410–440 Ma, which are consistent with the age of the Chingiz Arc. This suggests that the mafic rocks (ophiolitic components) in the Hebukesaier mélange were generated at a mid-ocean ridge and were later accreted to the Chingiz Arc, which formed above a southward-dipping subduction zone that consumed the Paleo-Asian Ocean. The predominant zircon age peaks of turbidites from the Saur area, north of the Hebukesaier mélange, range from 326 to 360 Ma, which areconsistent with a provenance from the Saur Arc. The distinctive detrital zircons of the Chingiz and Saur arcs indicate that the northern boundary of the Hebukesaier mélange is the tectonic boundary between the Chingiz and Saur arcs. We suggest that Paleo-Asian Ocean closed before Late Triassic as indicated by a diorite vein (ca. 218 Ma) that intruded the Hebukesaier mélange.

1. Introduction

Accretionary orogens, which are characterized by long-term subduction of oceanic crust, multiple amalgamations of exotic blocks, and juvenile island arcs, are well-known worldwide from the Archean to the Present (Cawood et al., 2009; Condie, 2007). The Altaids (the southern younger part of the Central Asian Orogenic Belt or CAOB) is the largest Phanerozoic accretionary orogen in the world. It was initially interpreted to have formed by subduction along a single long-lived magmatic arc (Şengör et al., 1993). However, more recently, it has been recognized that it consists of many accretional events that amalgamated ophiolites, microcontinents, island arcs, seamounts, and accretionary wedge materials (Wakita et al., 2013; Windley et al., 2007; Xiao et al., 2003, 2010, 2018, 2014, 2017; Figure 1a). The composition, structure, and age of these accretionary arcs, mélanges, and turbidites are crucial for understanding the spatial-temporal accretion process during the life of the Altaids (Şengör et al., 2018; Şengör & Natal'In, 1996; Wilhem et al., 2012; Xiao et al., 2018) .

The Kazakhstan orocline in the western Altaids is a significant part of the accretionary orogen (Kröner et al., 2007; Figure 1a). The Chingiz Arc (Chen et al., 2010; Coleman, 1989; Zhang et al., 2018) and the

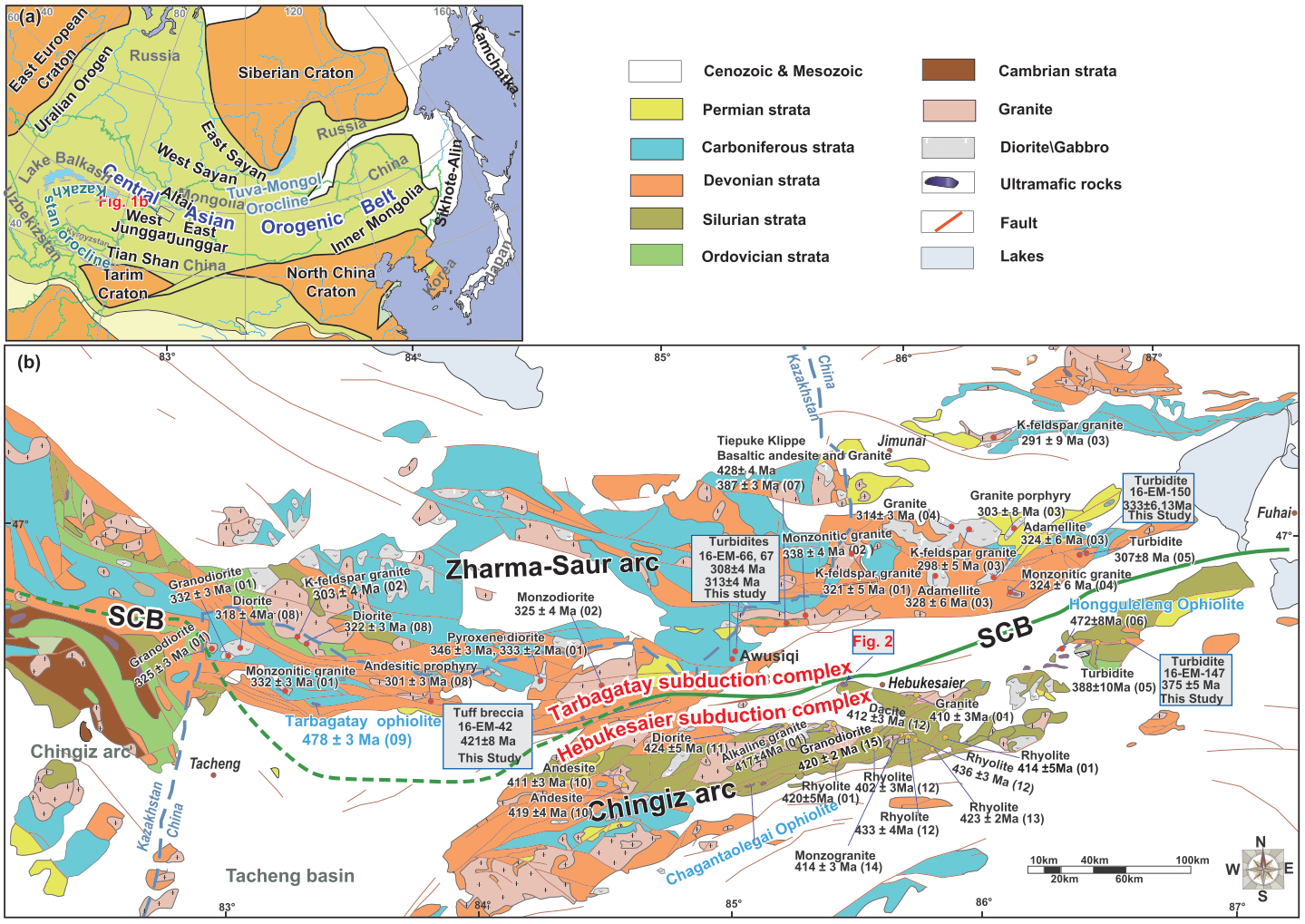

Figure 1. (a) Tectonic map showing the main collage systems of the CAOB, bound on the north by the Siberian (SC) and East European cratons (EEC) and on the south by the Tarim (TC) and North China cratons (NCC), modified after (Şengör et al., 1993; Wan et al., 2015; Xiao et al., 2010). (b) Simplified tectonic map of the Chingiz Arc, Saur Arc and the Chinese Altai (CA) showing their mutual boundaries, modified after (Chen et al., 2017a, 2017b). The location of the study area is indicated, and the ages of plutons and turbidites are marked. 01-(Chen et al., 2010), 02-(Han et al., 2006), 03-(Zhou et al., 2008), 04-(Yuan et al., 2006), 05-(Choulet, Faure, Cluzel, Chen, Lin, & Wang, 2012), 06-(Zhang & Guo, 2010), 07-(Zhang et al., 2015), 08-(Chen et al., 2017b), 09-(Zhu & Xu, 2006), 10-(Shen et al., 2012), 11-(Chen et al., 2015), 12-(Wang et al., 2014), 13-(Meng et al., 2010), 14-(Yin et al., 2018), 15-(Yin et al., 2017). SCB: Suar-Chingiz Belt which defines the Suar-Chingiz Arc Boundary.

Saur Arc (Chen et al., 2017b) are both located in the northern flank of the Kazakhstan orocline (Abrajevitch et al., 2008; Xiao et al., 2015). Both arcs contain evidence of the latest stage of the evolution in the West Junggar segment of the Altaids (Figure 1b). However, the subduction polarities and process of amalgamation of the two island arcs (Abrajevitch et al., 2007) remain enigmatic and controversial. For example, Choulet, Cluzel, et al. (2012), Luo et al. (2017), Shen, Pan, Shen, et al. (2015), and Shen et al. (2012) proposed that the Chingiz and Saur arcs were generated by southward subduction of the Irtysh Ocean, and the evolution of the two arcs was continuous. Alternatively, Chen et al. (2017b) proposed that the Chingiz Arc was generated by southward subduction, but that the Saur Arc was formed by northward subduction. The location of the suture between the Saur and Chingiz arcs, as well as the geological record and evolutionary history of the two arcs, is poorly understood. Here we focus on the Hebukesaier ophiolitic mélange that is located in the ophiolite-strewn belt between the two arcs (Zhang & Guo, 2010; Zhu & Xu, 2006; Figure 1b) as well as examining the detrital zircon record of turbidites (Chen et al., 2017a; Mutti et al., 2003; Mutti & Normark, 1987; Wang et al., 2006, 2018) that lie around the two arcs (Choulet, Cluzel, et al., 2012) in order to better constrain the age, the tectonic geography, and the evolution of this major part of the Altaids.

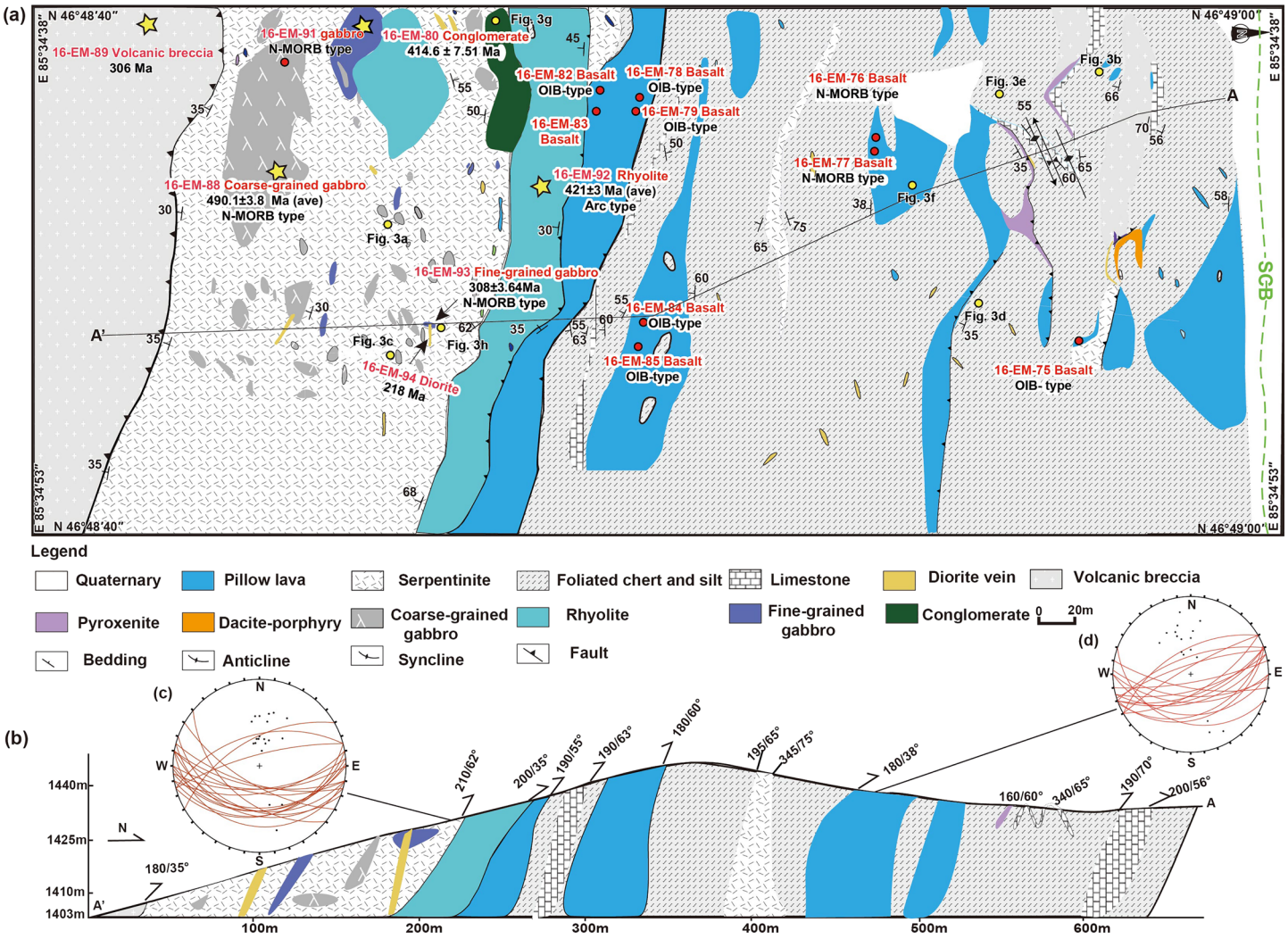

Figure 2. (a) A detailed field map of the Hebukesaier ophiolitic mélange showing the components of the mélange and locations of studied samples. (b) Cross-section from north to south in the Hebukesaier ophiolitic mélange.

To constrain the subduction polarity and major tectonic events of these two island arcs, we carry out field investigations along the Saur-Chingiz Belt (SCB) and map the Hebukesaier ophiolitic mélange and the surrounding turbidites (Figure 2). In this study, we discuss the different lithotectonic units of the SCB and evaluate the deformation history based on lithostructural mapping and structural analysis. We present new geochronological and geochemical data to constrain the tectonic nature of the ophiolitic rocks (Angiboust et al., 2013) and reassess the Hebukesaier ophiolitic mélange and the turbidites to better understand the final amalgamation of the southern Altaids.

2. Geological Setting

The Kazakhstan orocline comprises a pair of concentric horseshoe-shaped volcanic belts, which formed by the convergence of the cratonic blocks of Baltica, Siberia, and Tarim (Li et al., 2018; Safonova et al., 2017; Figure 1a). The Paleozoic orocline is divisible into a northern limb and southern limb, which connect with the Siberia and Tarim cratons, respectively (Xiao et al., 2015). Both the Bozshakol-Chingiz Arc (Ren et al., 2014; Shen, Pan, Shen, et al., 2015) and the Zharma-Saur Arc (Safonova et al., 2018) occur along the northern limb of the Kazakhstan orocline.

The Bozshakol-Chingiz Arc extends from Kokchetav in Kazakhstan to West Junggar in northwest China (Safonova et al., 2017; Şengör & Natal'In, 1996) and was mainly active from the late Silurian to

mid-Devonian (Chen et al., 2010; Shen et al., 2012; Figure 1b). The eastern Chingiz Arc in China (Abrajevitch et al., 2007; Abrajevitch et al., 2008; Chen et al., 2010; Shen et al., 2012) is surrounded by the Xiemisitai and Barleike Mountains in the south and separated from the Saur Mountains to the north. The main components of the Chingiz Arc include plutons (Chen et al., 2010, 2015; Wang et al., 2014; Yin et al., 2018), tholeiitic to calc-alkaline basalt, calc-alkaline andesite and dacite (Meng et al., 2010; Shen et al., 2012), and tuffaceous sedimentary rocks (Choulet, Faure, Cluzel, Chen, Lin, & Wang, 2012). The geochemical compositions of the volcanic and plutonic rocks indicate that they formed in a supra-subduction setting (Safonova et al., 2017; Shen, Pan, Seitmuratova, et al., 2015).

The Saur volcanic arc is located north of the Chingiz Arc. It extends over a distance more than 450 km from east Kazakhstan to NW China (West Junggar). The Saur Arc in the Tarbagatay Belt contains andesites, granitoid, and intrusive plutons (Chen et al., 2010; Han et al., 2006; Zhou et al., 2008), and tuffaceous sedimentary rocks associated with Carboniferous volcanic rocks (Choulet, Faure, Cluzel, Chen, Lin, & Wang, 2012). With its juvenile Hf-in-zircon isotopic characteristics and typical arc-related geochemical signatures (Chen et al., 2010; Hong et al., 2017), the Saur part of the Zharma-Saur Terrane is interpreted as a late Paleozoic volcanic arc (Cai, 1988; Chen et al., 2017a; Zhu & Xu, 2006; Figure 1b). The late Carboniferous sedimentary rocks of the Saur Arc are dominated by Devonian to Carboniferous detrital zircon grains (Li et al., 2017; Safonova et al., 2017), whereas the Boshchekul-Chingiz Arc contains abundant early Paleozoic detrital zircons (Choulet, Cluzel, et al., 2012).

The Saur and Chingiz arcs in NW China are separated by several ophiolites geographically: the Hongguleleng ophiolite (Zhang & Guo, 2010), the Chagantaolegai ophiolite (Zhao & He, 2014), the Tarbagatay ophiolite (Zhu & Xu, 2006), and the Saleinuohai ophiolite (Ren et al., 2014; Figure 1b). The existence of an oceanic basin between the Saur and Chingiz arcs is supported by gabbros that occur at Chagantaolegai (ca. 517 Ma) and Saleinuohai (ca. 516 Ma), which have an normal mid-ocean ridge basalt (N-MORB) geochemical signature (Chen et al., 2017a, 2017b; Han et al., 2006; Yang et al., 2018; Figure 1b).

3. Composition of the CSB

The SCB mainly consists of the ophiolitic mélange, the surrounding turbidites, and magmatic rocks related to Saur and Chingiz arcs. To get a better understanding of the SCB, we carry out detailed mapping to define the structure of the mélange. The exotic blocks in the mélange and the rocks interpreted as being a dismembered ophiolitic association were targeted to constrain the evolution of the Hebukesaier ophiolitic mélange. Samples of turbidites were collected for detrital zircon analysis to understand from which of the two arcs they were derived.

3.1. Structure of the Hebukesaier Ophiolitic Mélange

The Hebukesaier ophiolitic mélange mainly consists of serpentinite-matrix mélange with gabbro blocks found mainly in the south and chert-matrix mélange with pillow basalt-, limestone-blocks concentrated in the north. These lithologies are common tectonic layouts in other mélanges, such as the Jurassic accretionary complexes in Japan (Wakita, 2015; Wakita & Metcalfe, 2005), the Cretaceous Lycian mélange in Turkey (Collins & Robertson, 1997), and the serpentinite mélanges of the Franciscan subduction complex (Wakabayashi, 2012). Structures in the mélange include pinch-and-swell fabrics, shear zones, and imbrications, which are common in other mélanges such as the Solonker Ophiolitic Mélange (Fu et al., 2018), the Yeyagou ophiolitic mélange in West Junggar, NW China (Zhang, Xiao, Han, Ao, et al., 2011), and the McHugh Complex in the Kenai Peninsula of Alaska (Kusky et al., 1997).

The pinch-and-swell structures, a subset of boudins, occur where a more competent layer in a weaker matrix is subjected to the layer-parallel extension (Passchier & Trouw, 2005). At the outcrop scale, the competent chert and limestone blocks within a weaker cleavage chert matrix form the pinch-and-swell fabrics (Figure 5f), and their long axes are perpendicular to the shortening direction. Some local mélange outcrops occur asymmetric shear structures (Passchier & Trouw, 2005; Figures 5g and 5h). The clasts of the limestones (Figure 5g) and sandstones (Figure 5h) surrounded by the shear bands can be distinguished. The angular relationships and asymmetric configuration of the clasts and the incipient shear band structures suggest a bulk sinistral shear.

Imbricate thrust and fold structures are common compressional fabrics and well developed in this ophiolitic mélange. In the northern part, the basalts and cherts imbricate several times (Figure 2b). In the southern part, the volcanic breccia is in thrust contact with serpentinites in the south, with fault surface dipping south (Figure 2a). The shear zones indicate a south to north movement (Figures 5g and 5h). Besides, asymmetric folds in the cherts and limestones have southward dipping axial planes, implying (Figures 2b–2d) they are NWW-vergence folds. The imbricated thrusts, asymmetric folds, and movement direction of shear zones together suggest a top-to-the-N sense of shear.

3.2. Exotic Blocks in the Hebukesaier Ophiolitic Mélange

The Hebukesaier ophiolitic mélange crops out between the Saur Mountains and the Xiemisitai Mountains (Figure 2) and preserves different lithologies and compositions in its northern and southern ends (Figure 2a).

In the northern part of the mélange, there is a succession of cherts, pillow basalts, limestones, tuffs, plus fault-bound serpentinites. But in the southern segment, the mélange contains blocks of coarse- and fine-grained cumulate gabbro, conglomerate, and volcanic breccia (Du & Chen, 2017; Yang et al., 2018; Figure 2) in a serpentinite matrix. The mélange in the mapping area is intruded by veins of diorite. The serpentinites are in fault contact with pillow basalts and cherts. The pillow basalts are interbedded with cherts (Figures 3b and 3d) and limestones (Figure 2). Pillows that are about 30 to 80 cm across in their longest dimension are close-packed (Figure 3f). The basalts are porphyritic with plagioclase phenocrysts and vesicles filled with calcite (Figure 4d; Anonymous, 1972; Yang et al., 2015). Thin-bedded cherts (Figure 3e) contain recrystallized radiolaria that are indicative of pelagic deposition (Sugiyama, 1977; Figure 4g), some of which are highly deformed (Figures 2a and 5i). Folded limestones (Figure 2a) with south-dipping axial planes are interbedded with the chert and pillow basalts. Folds of the limestone are mainly open-tight, asymmetrical, upright with subvertical axial surfaces (Figure 2a), and their hinges are almost horizontal and strike NW-SE (Fu et al., 2018; Kusky et al., 2013; Safonova et al., 2016).

In the southern segment of the mélange, the serpentinite is widely distributed, heavily weathered and foliated (Figure 2a). The serpentinite (Figure 3c) contains relics of harzburgite and pyroxenite in which olivines are thoroughly altered, but primary mineral textures are preserved (Figure 4a; Luo et al., 2017). Blocks of coarse-grained gabbro (Figure 3c) consist of clinopyroxene (45–50%), plagioclase (50–55%), and minor amphibole; the pyroxenes and plagioclases are medium to coarse-grained (2 and 3 mm) and euhedral to subhedral (Figure 4b). These gabbros have cumulate textures and size-graded cumulate layering, which comprises alternating layers of anorthosite and melanocratic layers with pyroxene predominant. Fine-grained gabbros have no magmatic layering and consist of 0.2–0.25 mm grains of clinopyroxene (60%) that are surrounded by 1 and 2 mm plagioclase grains (40%; Figure 4c).

3.3. Coherent Sedimentary Rocks in the SCB

Coherent sedimentary rocks in the SCB are located in the surrounding area of the Kekesentao ophiolitic mélange and can be divided into two groups from their geographical positions. The sedimentary rocks in the Chingiz-Xiemisitai area are greywacke-dominant, showing coarse- to medium-grained graded bedding (Figures 5a and 5b). While in the Saur area, the sedimentary rocks preserve medium- to fine-grained Bouma sequences (Figures 5c–5e).

In the Chingiz area, the coherent sedimentary rocks are interthrust with the ophiolitic mélange (see Figure 1b). The greywackes south of the mélange have typical graded and convolute beddings overprinted by soft-sediment structures (Figure 5a). The sandstone interbedded with a conglomerate in the south of the mélange contains fragments of chert, gabbro, and sandstone (Figure 5b).

In the west Awusiqi (Saur Mountain) area (see Figure 1b), turbidites (16-EM-66 and 16-EM-67) show Bouma sequences with the fining upwards (Figure 5c). Turbidites (sample 16-EM-150) in the eastern Saur Arc exhibit rhythmic layers; the sandstone layers are interbedded with siltstone and mudstone layers (Figures 5d and 5e).

3.4. Other Rock Associations

A rhyolite block in the mélange (Yang et al., 2018; Figure 2) has thrust-contacts with pillow basalts and ultramafic rocks. Rhyolite (Figure 4f) has a porphyritic texture (Figure 4f) and triangular to elliptical, 2 and 3 mm

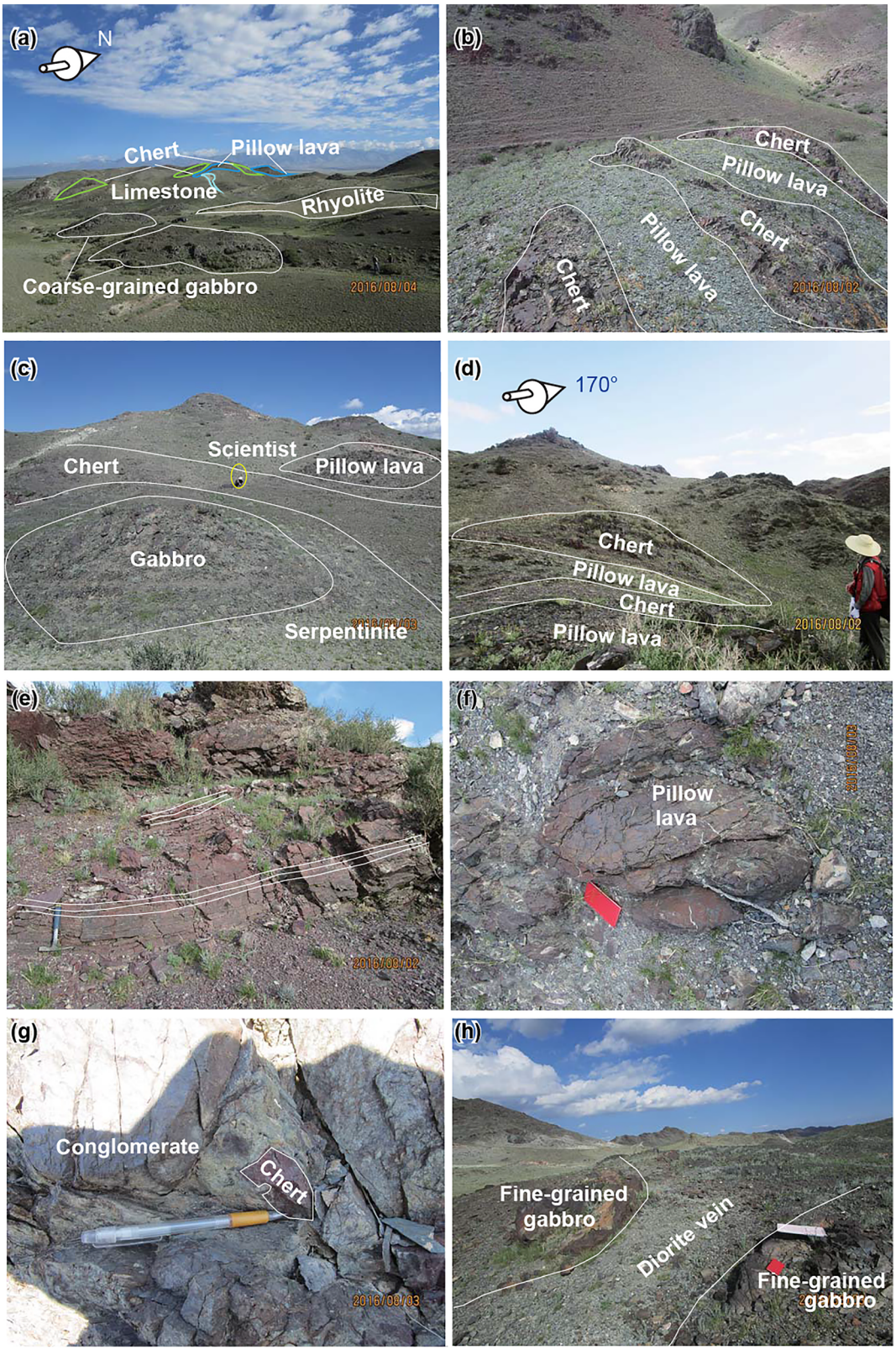

Figure 3. Photographs showing the field relationships of rocks of the ophiolitic mélange. (a) Overview of major components of the map area; (b) and (d) the relationships between cherts and pillow basalts bound by faults; (c) the relationships of the serpentinite, gabbro, chert, and pillow basalt; (e) thin-bedded red chert; (f) pillow basalts; (g) conglomerate containing chert clasts; (h) diorite vein intruding fine-grained gabbro.

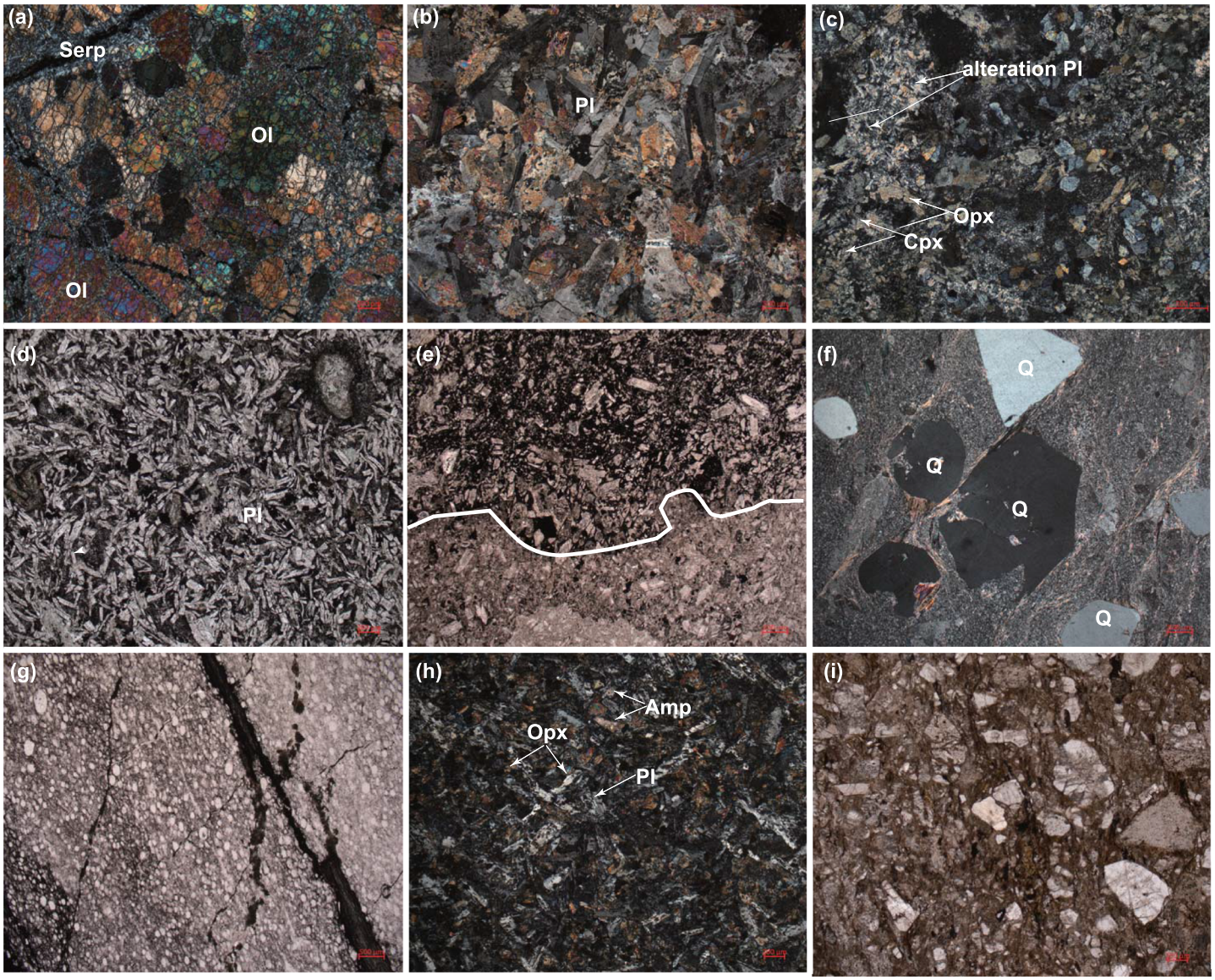

Figure 4. Microphotos of key rocks of the ophiolitic mélange. (a) Serpentinite (Sep) with olivine (Ol); (b) euhedral to subhedral plagioclase (Pl) crystals and clinopyroxenes (Cpx) in coarse-grained gabbro; (c) altered plagioclase (Pl) and clinopyroxene (Cpx) in fine-grained gabbro; (d) curved plagioclase (Pl) phenocrysts in pillow basalt; (e) boundary between two types of volcaniclastic rocks in volcanic breccia; (f) texture of rhyolite with quartz (Q) phenocrysts; (g) recrystallized radiolaria in chert; (h) amphibole (Amp) orthopyroxene (Opx), and plagioclase (Pl) in a diorite vein; (i) turbidite containing crystals of quartz and plagioclase.

quartz phenocrysts. Conglomerate in the southern part of mapping area is unconformable on serpentinites; 20–50 mm pebble clasts include serpentinite, gabbro, chert, and pillow basalt, which are all components of the ophiolitic mélange. The sharp-edge clasts indicate short-distance transport (Figure 3g). Volcanic breccias crop out mainly in the southernmost area, in fault contact with the ultramafic rocks. The breccias mainly consist of fragments of plagioclase detritus and minor clays (0.4 and 0.5 mm; Figure 4e). According to 1:200,000 maps, they are widespread in the ophiolite belt between the Saur and Chingiz arcs, where it is termed the Upper Devonian Tarbagatay Formation. Diorite veins, which have intruded the fine-grained gabbro of the Hebukesaier ophiolitic mélange (Figure 3h), consist of fine-grained amphibole, plagioclase, and pyroxene. The plagioclase is euhedral, ranging from 1 to 3 mm in size, and the amphibole forms acicular crystals that are 0.5 to 1 mm long (Figure 4h).

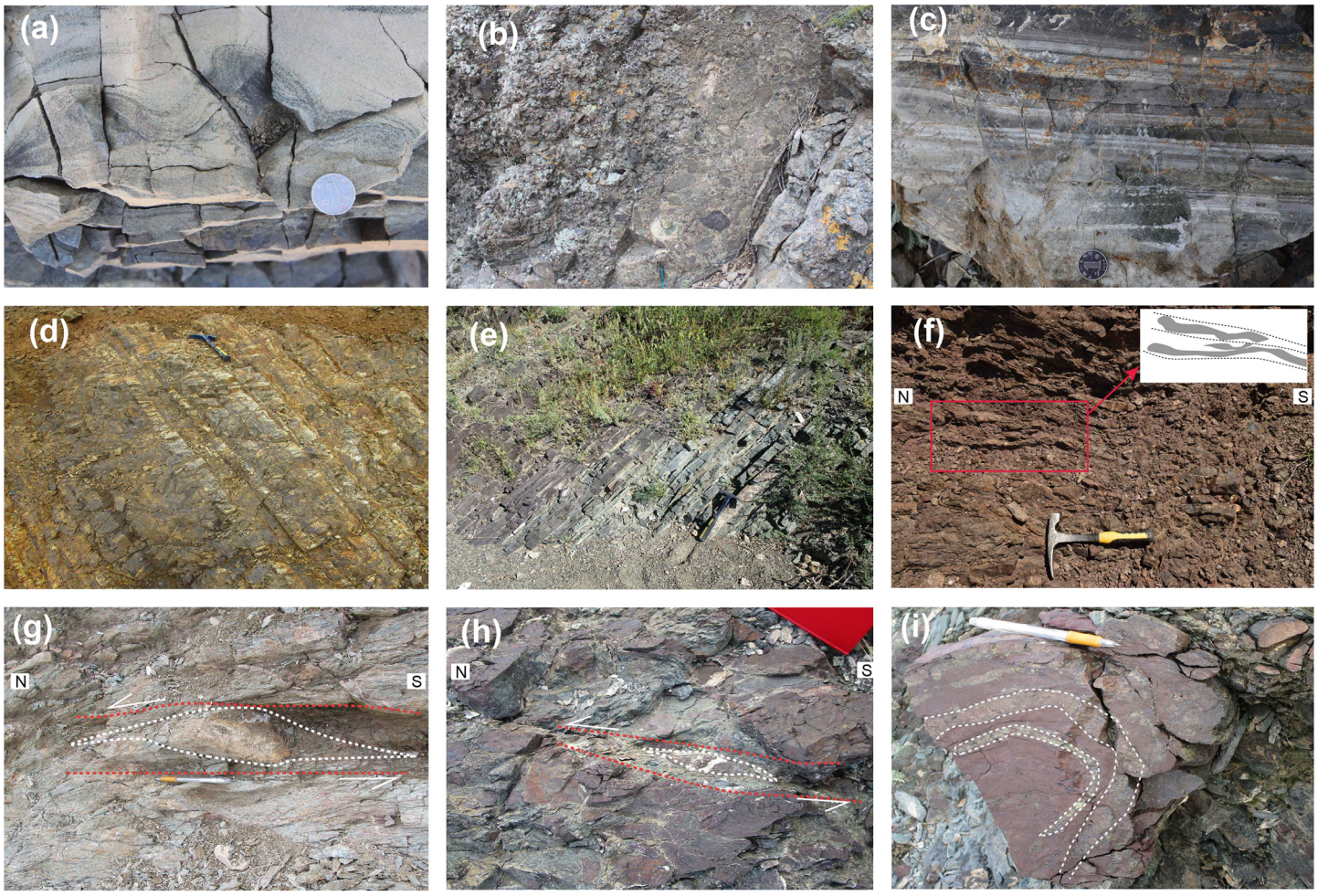

Figure 5. Outcrop photographs showing the turbidite of the Chingiz and the Saur area: (a) greywacke in the south of the mapping area, Chingiz area; (b) conglomerate in Chinigz area; (c) turbidite in the Awusiqi area, Saur area; (d) and (e) turbidite in Heishantou, Saur area; (f) pinch-and-swell structure in the thin-bedded chert; (g and h) photographs showing shear structures in the Hebukesaier mélange at outcrop scale; (i) folded chert in the Hebukesaier ophiolitic mélange showing the original bedding.

4. Methods

4.1. Zircon U-Pb Geochronology

Zircon concentrates from each rock were separated from 2–5 kg rock samples by conventional magnetic and density techniques to concentrate the nonmagnetic, heavy fractions. Zircon grains were mounted in epoxy resin and polished to expose their internal structures for analysis. Polished zircon grains were first examined by cathodoluminescence (CL) imaging on a CAMECA SX-50 microprobe at the Institute of Geology and Geophysics of the Chinese Academy of Sciences in Beijing. The operating conditions were 15 kV accelerating voltage and 19 nA beam current.

U-Pb dating and trace element analyses of zircons were simultaneously made with an LA-ICP-MS at the Wuhan Sample Solution Analytical Technology Co., Ltd., Wuhan, China. Detailed operating conditions follow Zong et al. (2017). Laser sampling was performed with a GeolasPro laser ablation instrument that consists of a COMPexPro 102 ArF excimer laser (wavelength of 193 nm and maximum energy of 200 mJ) and a MicroLas optical system. An Agilent 7700e ICP-MS instrument was used to acquire ion-signal intensities. Helium was applied as a carrier gas. Argon was used as the make-up gas and mixed with the carrier gas via a T-connector before entering the ICP. A “wire” signal smoothing device was included in this laser ablation system. The spot size of the laser was set to 32 μm. Zircon 91500 and glass NIST610 were used as external standards for U-Pb dating and trace element calibrations, respectively. Each analysis involved a background

acquisition of approximately 20–30 s followed by 50 s of data acquisition. An Excel-based software ICPMSDataCal was used to undertake off-line selection and integration of background and analyzed signals, time-drift corrections, and quantitative calibration for trace element analyses and U-Pb dating (Liu et al., 2010). Concordia diagrams and weighted mean calculations were made with Isoplot/Ex_ver3 (Ludwig, 2003).

4.2. Whole-Rock Major and Trace Elements

Seventeen powdered rock samples of ca. 200-mesh size were used for the chemical analyses. Major oxides were determined by wavelength dispersive X-ray fluorescence spectrometry (XRF) on fused glass beads using a SHIMADZU XRF 1500 spectrometer at the Australian Laboratory Services (ALS) Laboratory Group, Guangzhou. Loss of ignition (LOI) was determined after igniting a sample powder at 1000°C for 1 hr (Liu et al., 2008). Trace element abundances were measured on a Finnigan MAT element mass spectrometer (ICP-MS) at the ALS Laboratory Group after complete dissolution. Powders (40 mg) were dissolved in distilled HF + HNO3 in 15 ml Savillex Teflon screw-cap beakers at 200°C for five days, dried, and then diluted to 50 ml for analysis. Indium was used as an internal standard to correct for matrix effects and instrument drift (Pearce, 2008). Precision for all trace elements is estimated to be ±5%, and accuracy is better than ±5% for most elements using the GSR-2 standard (Workman & Hart, 2005).

5. Geochronological Data

Analyses were made of magmatic zircons in eleven samples of coarse-grained gabbros, fine-grained gabbros, rhyolites, conglomerates, volcanic breccias, and diorite veins, together with detrital zircons from turbidites surrounding the ophiolitic mélange. Sample locations are indicated in Figure 2a.

5.1. Exotic Rocks in the Hebukesaier Ophiolitic Mélange

The zircons from the coarse-grained gabbro sample (16-EM-88) in the Hebukesaier ophiolitic mélange (Figure 2) range from 80 to 180 μm in length (Figure 6). The zircons exhibit broad or weak oscillatory zoning in CL images with euhedral, sharp prisms, which is typical of the zircons crystallized from mafic magma. The length-width ratios are about 1.5:1, and the Th/U ratios of the zircons are 0.35–0.92 (0.63 average), suggesting a magmatic origin. A Wetherill Concordia diagram (Figure 7a) shows that the zircons have a weighted mean $^{206}Pb/^{238}U$ age of 490 ± 4 Ma (MSWD = 1.9), which we interpret as the time of crystallization of the gabbro.

The fine-grained gabbro sample (16-EM-93) is from the southern area. Zircon CL images show that the grain sizes range from 60 to 120 μm. Some zircons have weak zones while others are sector-zoned (Figure 6). The Th/U ratios vary from 0.18 to 2.41, indicating a magmatic origin. The thirty-four zircon grains yielded concordant ages ranging from 308 to 2,521 Ma, demonstrating a major population of mid-Ordovician (460 ± 2 Ma) zircons and subordinate Neoproterozoic (898 ± 6 Ma) and Paleoproterozoic (2,310 ± 18 Ma) age populations (Figure 7b). The youngest three grains (ca. 308–327 Ma) show typical core-rim structures (Figure 6), indicating the recrystallization of the zircons. They yield a weighted mean $^{206}Pb/^{238}U$ age of 318 ± 5 Ma, which we interpret as the best estimate of the crystallization age of the fine-grained gabbro. The early Cambrian to Ordovician ages are consistent with the activity of the Chingiz Arc. In contrast, the subordinate Proterozoic peaks at 2,310 and 898 Ma are similar to those reported in the Kazakhstan terrane (Kokchetav) that shared the same trench as the Chingiz Arc in the early Paleozoic (Degtyarev & Ryazantsev, 2007; Li & Poliyangsiji, 2001).

5.2. Turbidites in the SCB

Several turbidite and breccia samples were chosen for LA-ICP-MS zircon dating to understand their provenance. Zircon grains from the turbidite (sample 16-EM-147) range from 80 to 150 μm in length and have length-width ratios of 1.5:1 to 3:1. Most grains show magmatic oscillatory zones. Some grains show sector zones in CL with the Th/U ratios falling in the range of 0.06–0.93. Forty-eight points give $^{206}Pb/^{238}U$ ages that range from 375 to 603 Ma (Figure 9a). The primary age peak ranging from 410 to 490 Ma is close to that of the Chingiz Arc, and the youngest age of 375 ± 5 Ma constrains the maximum age of deposition. Zircon grains from a tuff breccia (16-EM-42) range from 50 to 100 μm in length and have magmatic oscillatory to sector zones with the Th/U ratios of 0.21–0.87. Forty points give U-Pb ages ranging from 421 to 523 Ma

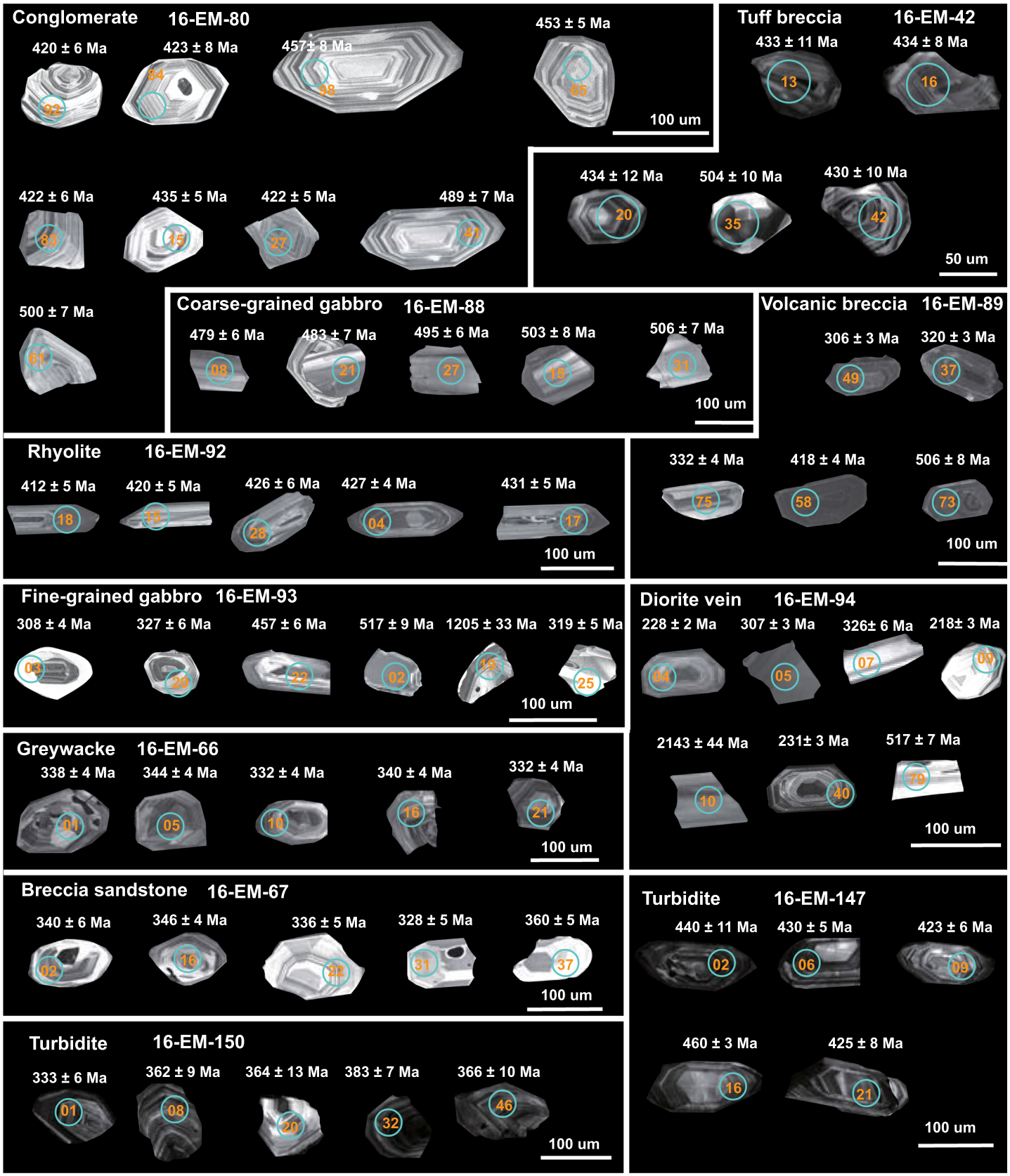

Figure 6. CL images of analyzed zircons from turbidites and plutons in the mélange.

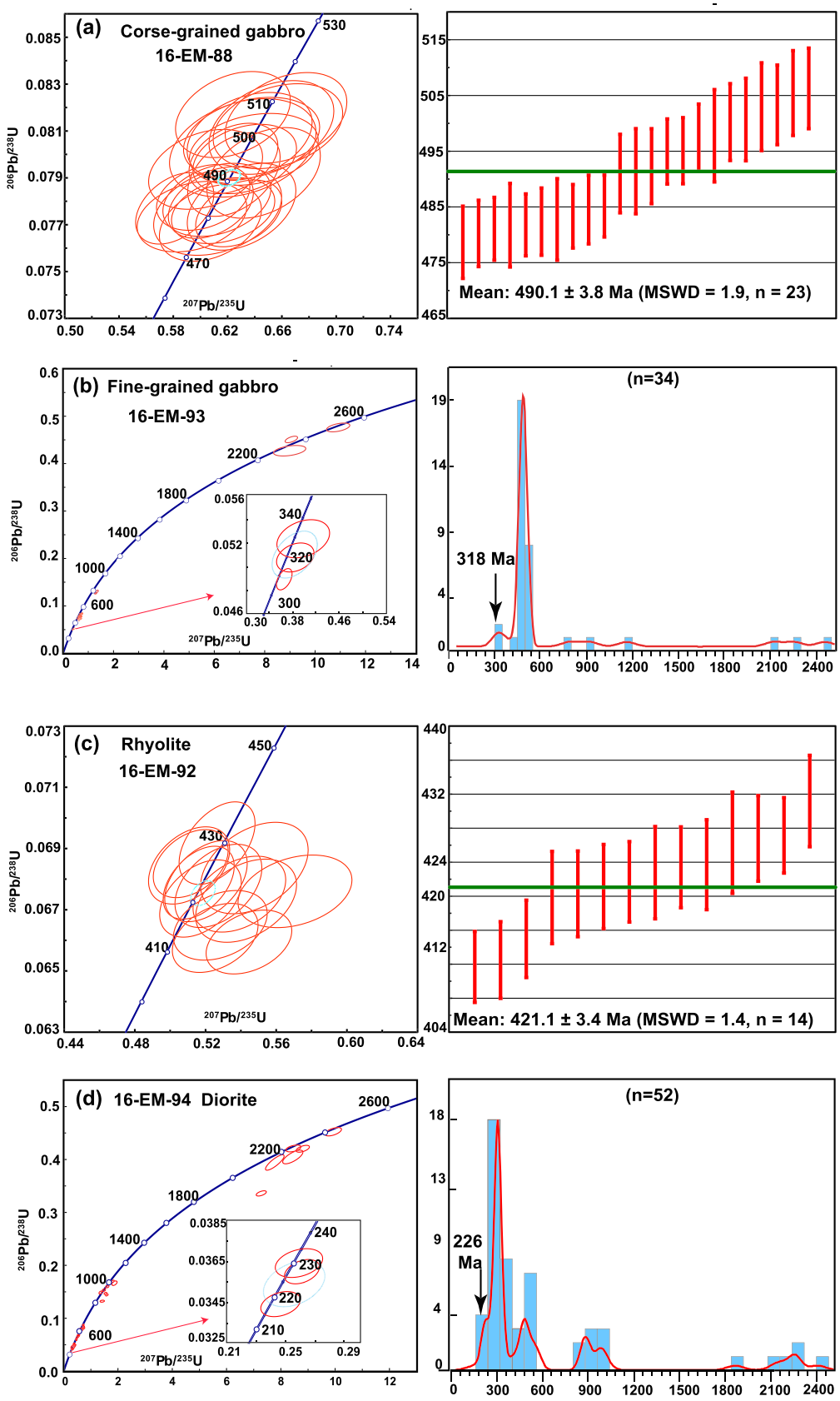

Figure 7. Zircon isotope diagrams of (a) coarse-grained gabbro; (b) fine-grained gabbro; (c) rhyolite; and (d) diorite.

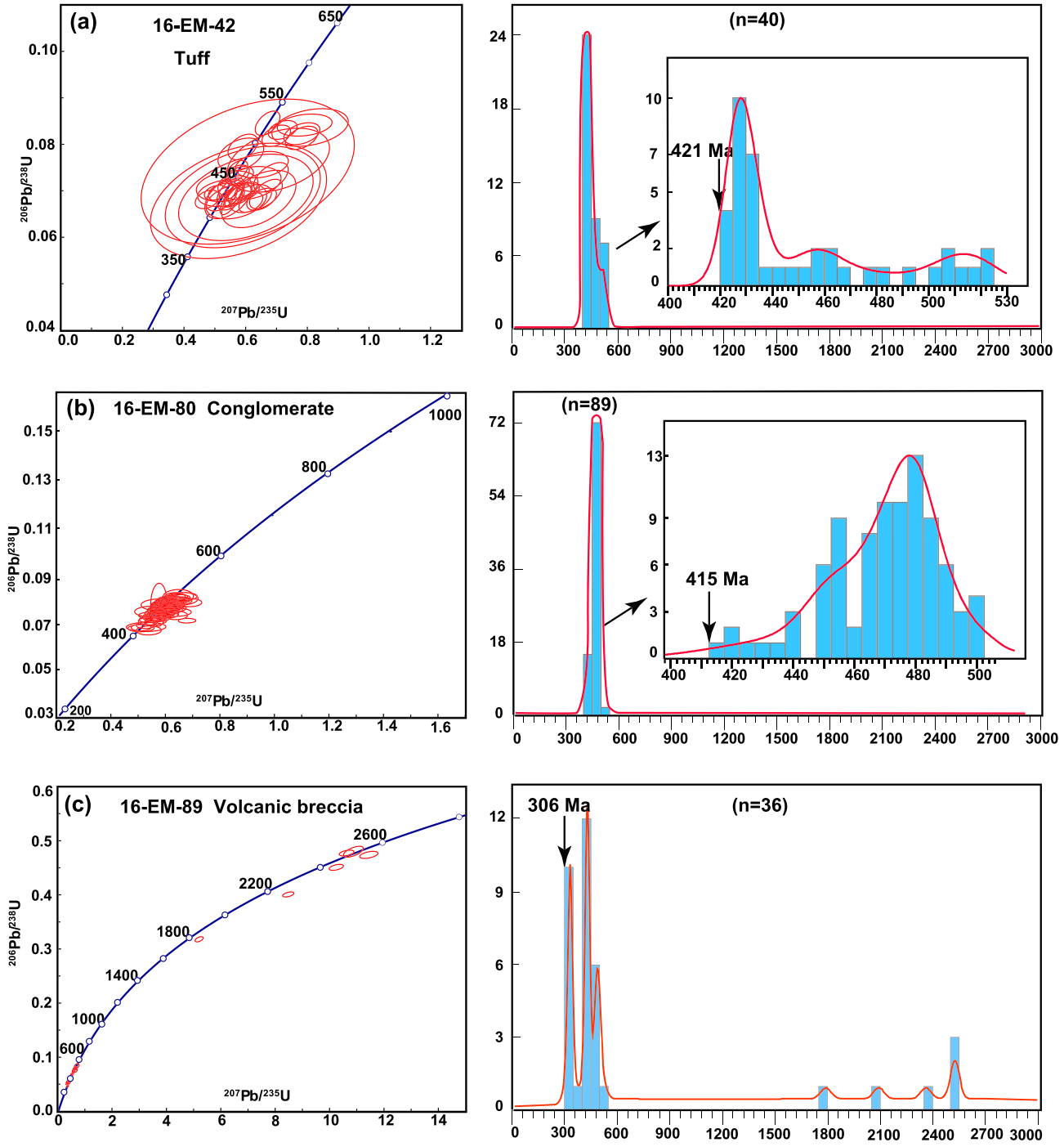

Figure 8. Zircon age diagrams of (a) tuff breccia (16-EM-42); (b) conglomerate (16-EM-80) in the Hebukesaier ophiolitic mélange; and (c) volcanic breccia (16-EM-89).

(Figure 8a), consistent with the magmatic activity of the Chingiz Arc. The youngest age indicates that the age of deposition was no earlier than 421 ± 8 Ma.

Zircon grains of samples 16-EM-66, 16-EM-67, and 16-EM-150 from the Saur area range from colorless to brown and have lengths of 50–150 μm. The length-width ratios vary from 1.2:1 to 2.5:1. Some zircon grains show oscillatory zones, whereas some are weakly zoned on CL images, and their Th/U ratios are in a range of 0.24–1.72. A total of 240 zircons were analyzed; 225 grains yielded concordant ages ranging from

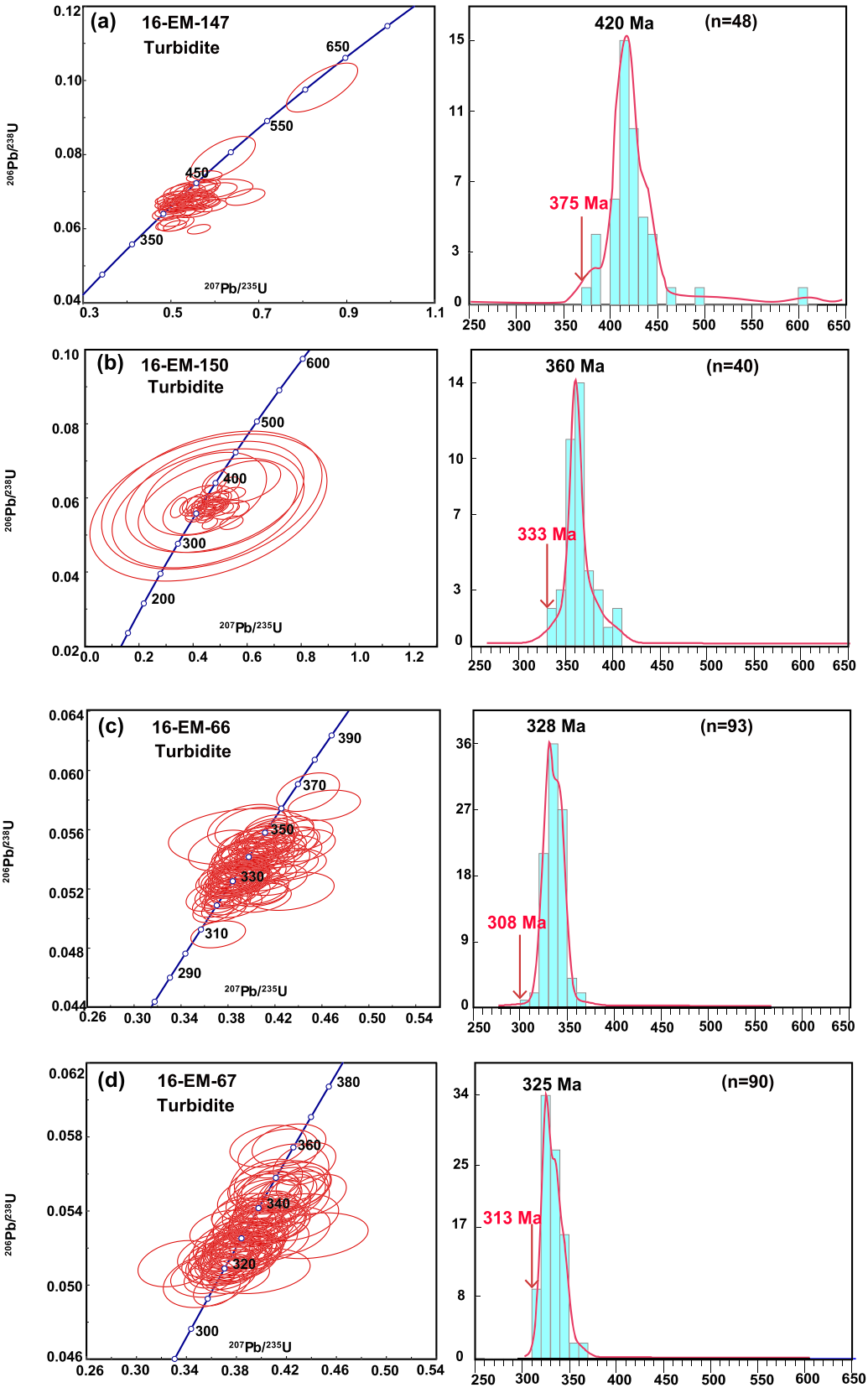

Figure 9. Detrital zircon ages of (a) turbidite (16-EM-147); (b) turbidite (16-EM-150) in the Chingiz area; (c) turbidite (16-EM-66); and (d) turbidite (16-EM-67) in the Saur area.

308 ± 4 Ma to 402 ± 23 Ma. Zircons from samples 16-EM-66 and 16-EM-67 define an age peak of ca. 326 Ma, and sample 16-EM-150 provides an age peak of 360 Ma (Figures 9b–9d). Similar early Devonian to middle Carboniferous age populations were widely reported in the Saur Arc area (Chen et al., 2017a, 2017b; Choulet, Faure, Cluzel, Chen, Lin, Wang, & Jahn, 2012).

5.3. Other Rock Associations

The zircons in the rhyolite sample (16-EM-92) range from 120 to 180 μm in length and have a length-width ratio of 3:1. The euhedral to subhedral grains have distinct magmatic oscillatory zones (Figure 6) and Th/U ratios of 0.19–0.54 (0.32 on average). These features suggest a magmatic origin. Fourteen spots on these zircons or zircon fragments yielded a weighted $^{206}Pb/^{238}U$ mean age of 421 ± 3 Ma (MSWD = 1.4) on the Wetherill Concordia diagram (Figure 7c), which we consider to be the crystallization age of the rhyolite. This age is close to the primary period of the Chingiz Arc.

Zircons from the conglomerate sample (16-EM-80) in the matrix of the southern mélange range from 60 to 180 μm and have a variety of structures. Some show magmatic oscillatory zones, whereas others are sector-zoned or only weakly zoned. The Th/U ratios are in the range of 0.26–1.00 (Figure 6). The $^{206}Pb/^{238}U$ ages range from 415 to 500 Ma (Figure 8b). The youngest zircon U-Pb age is 415 ± 8 Ma, which is consistent with the age of the rhyolite (Du & Chen, 2017; Luo et al., 2017; Yang et al., 2018).

The volcanic breccia sample (16-EM-89) is from the southern part of the mapped area. The 36 analyzed zircons are euhedral to subhedral and exhibit broad or weak oscillatory zones (Figure 6) with Th/U ratios of 0.04–1.69. The zircons show a wide range in $^{206}Pb/^{238}U$ ages between 306 and 2,560 Ma with age-peaks at 320, 420, 490, and 2,500 Ma (Figure 8c). Similar-aged Precambrian zircons (1,853–2,513 Ma) were also reported in the Kazakhstan area (Degtyarev & Ryazantsev, 2007). The early Paleozoic age clusters of 420 and 490 Ma record events in the history of the Chingiz Arc (Du & Chen, 2017; Yang et al., 2018), and the youngest 306 ± 3 Ma age constrains the maximum age of deposition.

Diorite veins (16-EM-94) intruded into most of the components of the mélange. Their zircon grains are euhedral to subhedral and have a length of 50–120 μm. On CL images, most grains show oscillatory to sector zones with the Th/U ratios ranging from 0.09 to 1.21, indicating a magmatic origin. Fifty-two analyzed spots give $^{206}Pb/^{238}U$ ages that range from 218 to 2,428 Ma (Figure 7d). The youngest three grains (ca. 218–231 Ma) show magmatic sector zones and yielded a weighted mean $^{206}Pb/^{238}U$ age of 226 ± 3 Ma, which we suggest is the best estimate of the crystallization age of the diorite.

6. Whole-Rock Geochemistry

The resultant major and trace element measurements are shown in Table S1 in the supporting information. We will present below a brief discussion about the chemical character of the key rocks of the Hebukesaier ophiolitic mélange.

6.1. Pillow Basalt

The pillow basalt samples show high SiO_2 and TFe_2O_3 values of 39.09–46.59 wt.% and 8.39 to 14.22 wt. %, respectively, and low TiO_2 of about 1.47 wt.% to 3.24 wt.% and MgO values (1.73–9.31 wt.%). The total REE contents range from 31.79 to 292.35 ppm, and the total content of LREE is 19.05–252.48 ppm.

The basalt samples are divisible into three groups. Group I shows slightly depleted LREE-enriched patterns ($(La/Yb)_N$ = 0.68–0.76), similar to those of an N-MORB. Group II displays moderate LREE-enriched patterns ($(La/Yb)_N$ = 2.69–3.06), similar to an enriched mid-ocean ridge basalt (E-MORB). Group III shows strong LREE-enriched patterns ($(La/Yb)_N$ = 7.98–18.22), and the fractionated trend is similar to that of ocean island basalts (OIB, Figures 10c and 10d).

On a primitive mantle-normalized spider diagram, Group I shows prominent positive Sr anomalies, whereas Groups II and III have prominent negative Sr anomalies. All the three groups display mildly positive Ta anomalies and positive Ti anomalies except for sample 16-EM-75, which has negative Ti anomalies (Figure 10d).

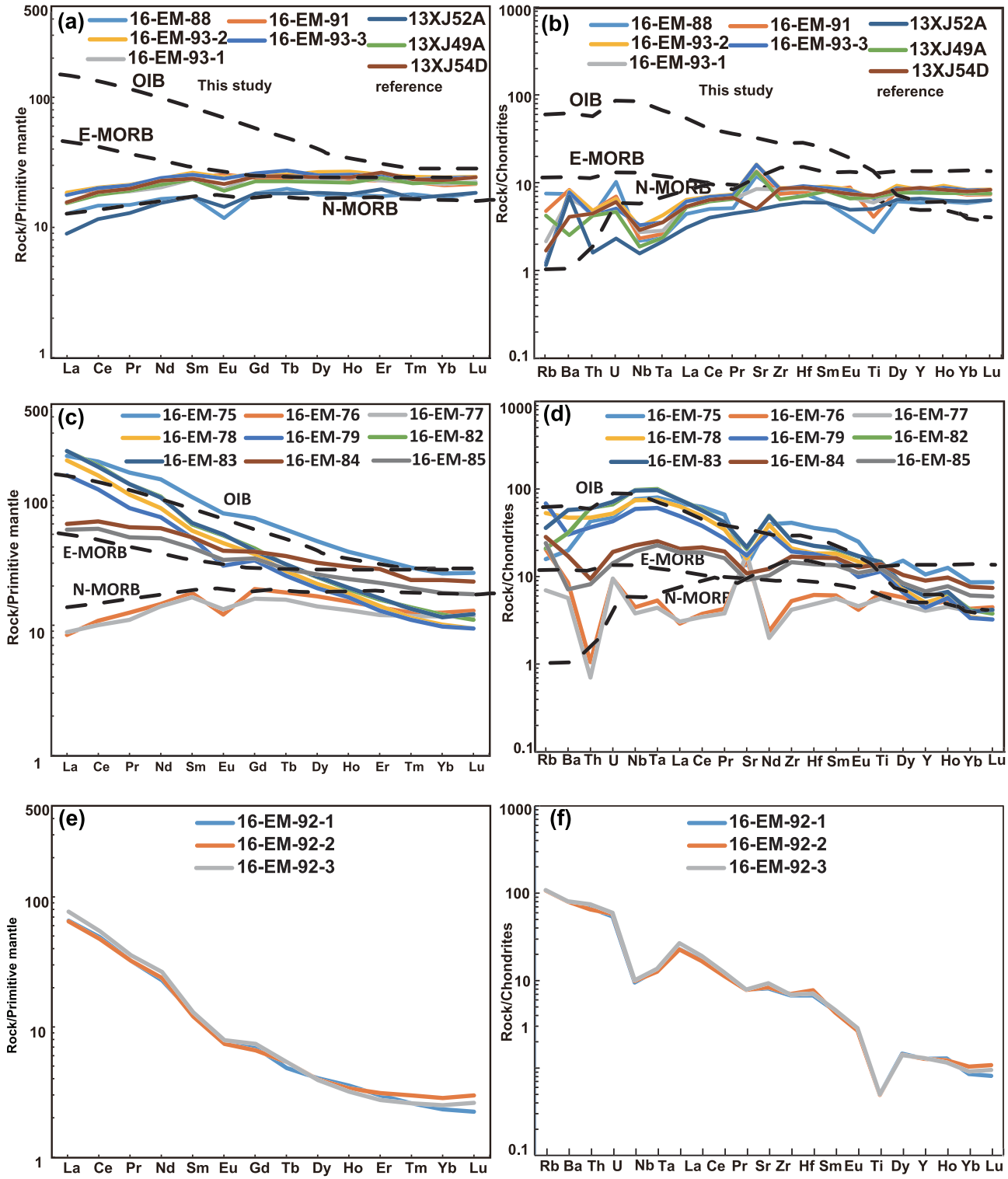

Figure 10. Chondrite-normalized REE patterns (a, c, e) and primitive mantle (PM)-normalized multielement diagrams (b, d, f) of gabbro, pillow basalt and rhyolite of the Hebukesaier ophiolitic mélange. In (a) and (b) gabbro samples EM-88, 16-EM-91, 16-EM-93-1, 16-EM-93-2, and 16-EM-93-3 are from this study, and 13XJ49A, 13XJ52A, and 13XJ54D are from Du and Chen (2017); In (c) and (d) pillow basalt diagrams, 16-EM-75 to 16-EM-79, 16-EM-82 to 16-EM-85 are from this study; In (e) and (f) rhyolites, 16-EM-92-1, 16-EM-92-2, and 16-EM-92-3 are from this study. The chondrite, PM, N-MORB, E-MORB, and OIB values are from Sun and McDonough (1989). Abbreviations: N-MORB, normal mid-ocean ridge basalt; E-MORB, enriched mid-ocean ridge basalt; OIB, oceanic island basalt.

6.2. Coarse-Grained Gabbro

The coarse-grained gabbro samples display high SiO_2 and TFe_2O_3 values of 53.46 to 54.12 wt.% and 8.77 to 11.28 wt.%, respectively, and low TiO_2 values of 0.63 to 0.93 wt.% and MgO values of 4.79 to 6.76 wt.%. Chondrite-normalized REE patterns are nearly flat, for example, $(La/Yb)_N = 0.75–0.86$, and show no striking Eu anomalies ($\delta Eu = 0.67–1.07$), suggesting a residue of plagioclase in the magma chamber (Figure 10a). In the primitive mantle-normalized spider diagram for trace elements, the gabbros show negative Th and Nb anomalies and Sr enrichments (Figure 10b).

6.3. Fine-Grained Gabbro

SiO_2 values of the fine-grained gabbro samples lie between 40.57 and 43.88 wt.% and the TiO_2 values between about 1.40 and 1.50 wt.%. The fine-grained gabbro also has high TFe_2O_3 (13.06–13.88 wt.%), MgO (6.48 to 6.58 wt.%). The total REE contents (ΣREE) are relatively high (from 53.87 to 60.96 ppm). Chondrite-normalized REE patterns are nearly flat, for example, $(La/Yb)_N = 0.72–0.76$ and display no obvious Eu anomalies ($\delta Eu = 0.81–0.93$; Figure 10a). On primitive mantle-normalized diagrams, the trace elements show negative Th, Nb, Ta, P, and Ti anomalies, and the Ba and Sr are enriched. Accordingly, the fine-grained gabbro is similar to N-MORB (Figure 10b).

6.4. Rhyolite

The rhyolite samples display extremely high SiO_2 values of 72.54–72.62 wt.% and low TiO_2, MgO, and TFe_2O_3 values of 0.09–0.13 wt.%, 0.40–0.45 wt.%, and 1.65–1.66 wt.%, respectively. The total REE contents of the rhyolite range from 66.28 to 75.40 ppm, while the content of LREE (62.19–71.30 ppm) is much higher than the HREE content (4.04–4.10 ppm), with ΣLREE/ΣHREE ranging from 15.21 to 17.39.

The chondrite-normalized REE patterns show high LREE-enriched values ($(La/Yb)_N$=21.94–29.49, Figure 10e). Primitive mantle-normalized trace element patterns show distinctive negative Nb, Sr, P, and Ti anomalies, and Nd, La, Hf, and Y enrichments, indicating that the rhyolite was formed in a subduction-related setting (Figure 10f), which is in agreement with the results of Yang et al. (2018).

7. Discussion

The evolution of the Hebukesaier ophiolitic mélange and the related arcs is important to understand the accretionary processes of the southern Altaids (Windley & Xiao, 2018). Our structural, geochronological, petrological, and geochemical data of the SCB provide evidence for the origin of the ophiolite and the long-term tectonic evolution of the surrounding blocks.

7.1. Origin of the Hebukesaier Ophiolite

7.1.1. Petrogenesis and Tectonic Setting of the Basalts

Discrimination diagrams and spider diagrams of the geochemical characteristics of volcanic rocks in an ophiolite are considered to be useful for the identification of tectonic settings (Liu et al., 2008; Pearce, 2008; Pearce et al., 1997; Pearce & Cann, 1973).

The basalts from the Hebukesaier ophiolite show high LOI mostly of 2.89–6.84 wt.% (except two samples up to 10.63 and 11.84 wt.%, respectively), which probably resulted from postmagmatic hydrothermal activity, which is commonly recorded by chlorites and some carbonate veins. The alteration may have mobilized the major elements and some LILEs such as Rb, Sr, Th, Ba, Eu, and U, which is reflected in their wide variation in our rocks (Table S1). Most "immobile" elements, especially high-field strength elements such as Nb, Ta, Zr, Hf, and Y are resistant in the alteration process (Pearce, 2014; Pearce & Peate, 1995; Pearce, 2008; Pearce & Cann, 1973). As a result, only the immobile incompatible trace elements and the REE are considered in the following discussion on the tectonic setting.

The Group I samples show depleted LREE-enriched patterns, but no anomalies in the high-field strength elements (e.g., Ta, Zr, and Hf), as illustrated in the chondrite-normalized REE and primitive mantle-normalized trace-elements patterns (Figures 10c and 10d). These relations strongly indicate that Group I pillow basalts formed in an N-MORB tectonic setting. The Group II samples display a slight enrichment in LREEs, but no obvious Nb, Ta, and Ti anomalies; these relations are similar to those of E-MORB. The Group III samples show strong enrichment in LREEs, suggesting an OIB setting (Figure 10c). The ratios of trace elements with different fractionation can provide valuable information

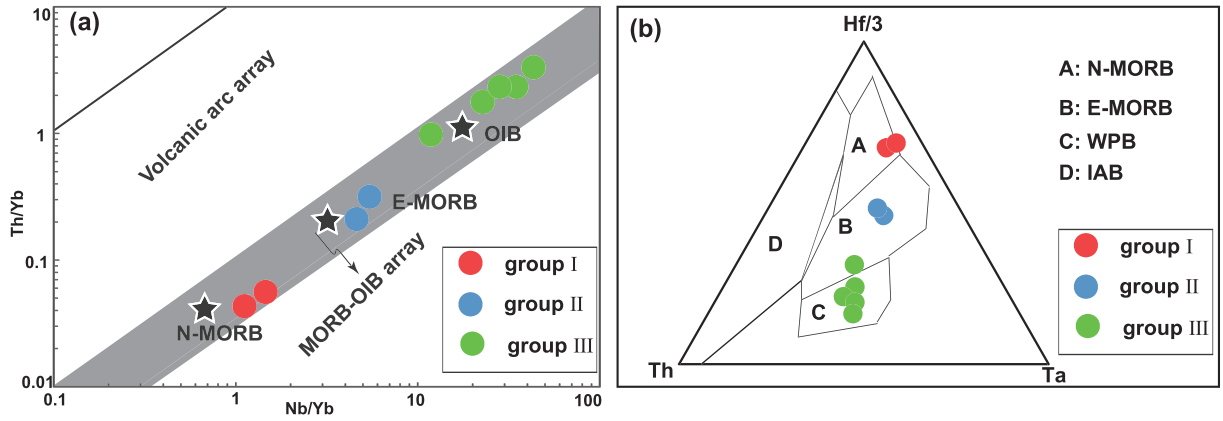

Figure 11. Petrochemical diagrams of pillow basalts from the Hebukesaier ophiolite: (a) Th/Yb-Nb/Yb discrimination diagram; (b) Th-Hf-Ta discrimination diagram (Wood, 1980).

on the petrogenetic history. On a Nb/Yb-Th/Yb diagram and a Hf/3-Ta-Th diagram, the ratios of the immobile incompatible trace elements, like Th, Nb, Yb, Ta, and Hf in the Groups I and II samples, lie in, or near, the fields of N-MORB and E-MORB, respectively. This permits us to conclude that these two groups were derived from a spreading oceanic ridge and sourced from a mantle plume or an enriched area in the upper mantle. In contrast, the ratios of Group III rocks are consistent with the feature of the OIB or within plate basalt (WPB), indicate that the Group III basalts were derived from an oceanic island, which is consistent with their accretion to the mélange during a subduction-accretion process (Figures 11a and 11b).

7.1.2. Petrogenesis and Tectonic Setting of the Gabbros

The gabbros from the Hebukesaier ophiolite show high LOI mostly of 2.25–6.07 wt.% (except one sample down to 0.66 wt.%), which probably resulted from alteration caused by postmagmatic hydrothermal activity. The alteration can be demonstrated by the large-variation of Na_2O (0.36–5.23 wt.%), Rb (0.80–4.90 ppm), and Sr (183.5–350 ppm) contents (see Table S1). Because the high-field strength elements such as Nb, Ta, Zr, Hf, and Y are resistant, the immobile incompatible trace elements and the REE are used in the following discussion.

The gabbros display significant negative Eu anomalies, indicate that plagioclase fractionation played an essential role in the magmatic evolution. The low Th and U contents and ratios of Th/U (1.68–3.36), Th/Yb (0.09–0.13), Rb/La (0.18–1.58), and high ratios of Ce/Nb (5.25–7.18), Nb/Ta (12.78–16.67), and Y/Nb (15.83–21.59) of the gabbro samples suggest that the magmas were possibly derived from a depleted mantle source, which can be reflected by the lack of anomalies in high-field strength element (e.g., Ta, Zr, and Hf). Those characteristics are similar to those of N-MORB. This conclusion is supported by the depleted LREE in chondrite-normalized REE distribution patterns (Figure 10a) and the nondifferentiation of HFSE in primitive mantle-normalized trace-elements patterns (Figure 10b). The scattered U-Pb zircon ages in the fine-grained gabbro sample are consistent with those of the other gabbros. Postmagmatic hydrothermal activity, which is commonly recorded by chlorites and some carbonate veins, may have mobilized the major elements and some LILEs such as Rb, Sr, Th, Ba, Eu, and U, which can be reflected in their wide variation in our rocks (Table S1).

The geochemical tectonic discriminants, chondrite-normalized REE, and primitive mantle-normalized trace element signatures together with field relations in the ophiolite suggest that the ophiolite was generated in a mid-ocean ridge setting. While the basalts with OIB characteristics were probably formed in seamounts (oceanic islands/plateaus). The formation of the OIB-type basalts is considered as the result of the activities of the mantle plume (Du & Chen, 2017; Yang et al., 2018). With the evolution of the ocean in Chingiz area, the seamounts was carried along by plate motions and eventually accreted to accretionary complex in Chingiz area, contributing to the components of the Hebukesaier ophiolitic mélange.

7.2. Subduction Polarity

Although Shen et al. (2012) and Zhao and He (2014) put forward the idea that the Chingiz Arc was generated by southward subduction; the evolutionary history of the SCB has been weakly constrained. Accordingly, our structural analysis and U-Pb zircon data of the key components of the ophiolitic mélange can provide usefully, and indeed diagnostic, constraints of the polarity of subduction.

The Chingiz and Saur arcs experienced long-term, multiple subduction and deformation. Previous studies suggest that subduction polarity can be indicated by the vergence of the imbrication system, such as the northward subduction of the Saur Arc (Chen et al., 2017b) and the West Junggar arc (Zhang, Xiao, Han, Mao, et al., 2011). Planar structures such as foliations, axial planes of asymmetric folds, and the relevant thrust faults consistently strike nearly E-W and dip to the south. The asymmetric folds developed in the accretionary wedge indicate top-to-the-north movement direction. The kinematic indicators suggest a southward subduction polarity of the oceanic plate.

Besides, the rhyolite which is thrust-imbricated with other components of the ophiolite has a crystallization age of 421 ± 4 Ma, corresponding to the magmatic age of the Chingiz Arc. The conclusion is also supported by the subduction-related geochemical features (Figures 10e and 10f). The detrital zircon ages of greywacke (Figure 9a), tuff (Figure 8a), and conglomerate (Figure 8b) have predominant age populations at 420, 480, and 530 Ma, respectively, consistent with the age of the Chingiz Arc located south of the Hebukesaier ophiolitic mélange (Chen et al., 2010; Shen et al., 2012; Xiang et al., 2015; Yin et al., 2017; Zhang et al., 2018). In addition, the angular grain shapes of clasts in the conglomerate and the zircon morphologies of the sediments in the mélange imply a short transportation distance, together indicating that the Chingiz Arc is the most likely provenance of the sedimentary rocks in the Hebukesaier mélange. In contrast, the Silurian-Ordovician age population is absent in the Saur area located to the north of the subduction complex.

The kinematics and the provenance analysis together suggest the evolution of Hebukesaier ophiolitic mélange is related to the southward subduction in the Chingiz area.

7.3. Evolution of the Chingiz Arc

The crystallization age of the coarse-grained gabbro was 490 ± 4 Ma, consistent with the gabbro SHRIMP U-Pb zircon age of 472 ± 8 Ma (Zhang & Guo, 2010) in the Hongguleleng ophiolite, and the LA-ICP-MS zircon U-Pb age of 517 ± 3 Ma (Zhao & He, 2014) of gabbro in the Chagantaoluogai ophiolite in the SCB. The N-MORB ophiolite indicates that an ocean existed in the Chingiz-Xiemisitai area during the late Cambrian to early Ordovician.

The LA-ICP-MS zircon U-Pb age of fine-grained gabbro, which exhibits the N-MORB geochemical signature, ranges from 308 ± 4 to 2,521 ± 26 Ma. The best estimation of the crystallization age can be identified from the youngest three zircon grains of 318 ± 5 Ma (Figure 7c), which show typical core-rim structures (Figure 6). The volcanic breccias of the mélange were thrust onto serpentinites, and their detrital zircon ages range from 306 ± 3 to 2,513 ± 20 Ma with peaks at ca. 320, 420, 490, and 2,500 Ma. A zircon age population of 404–506 Ma is consistent with the age of the Chingiz Arc, the smaller age peak of 320 Ma is consistent with the upper Carboniferous zircons of gabbro. The presence of fine-grained gabbro (ca. 318 Ma) with MORB-like geochemical characteristics in the Hebukesaier mélange indicates that the spreading of the oceanic crust continued to the late Carboniferous.

In the Saur area, the maximum depositional age determined by detrital zircons (ca. 262 Ma; Chen et al., 2017a) indicates that deposition of the tuff-bearing turbidites lasted until early Permian time. The conclusion is supported by the coeval fossils in the turbidites, including Michelinia, Meniscophyllum. This may constrain the lower age for subduction beneath the Zharma–Saur Arc. The diorite veins intruded the Hebukesaier ophiolitic gabbro, serpentinite, and other components of the melange. The diorite contains xenocrysts and show core-rim structures in CL images (Figure 6), indicating the recrystallization of the zircons. The youngest three zircon U-Pb ages (ca. 218–231 Ma) were obtained from the rim of the zircons and yielded a weighted mean $^{206}Pb/^{238}U$ age of 226 ± 3 Ma (Figure 7d), which we suggest is the best estimate of the crystallization age of the diorite. This late Triassic crystallization age of the diorite provides the time of termination of subduction in the Chingiz Arc (Xiao et al., 2015, 2018).

7.4. The Boundary Between the Chingiz and Saur Arcs

The detrital zircon-bearing turbidite (16-EM-66, 16-EM67) is located 10 km to the north of the Hebukesaier ophiolitic mélange. Prior researchers considered that the turbidite was deposited in the Late Devonian (360–372 Ma; Chen et al., 2017a). The youngest detrital zircon in these turbidites is 308 ± 4 Ma, suggesting that deposition of the turbidites in the Saur Arc area continued until at least the Late Carboniferous. The zircon age peak and the maximum deposition age of the turbidite (DJ-329; Choulet, Cluzel, et al., 2012) located in the east of the mélange are ca. 330 and 307 Ma, respectively. The andesite from northwest of the Hebukesaier ophiolite mélange has a concordant age of 326 ± 2 Ma (Chen et al., 2017b), which represents the time of major activity of the Saur Arc. The turbidite (16-EM-150) from the eastern part of the Saur area has detrital zircon ages ranging from 333 to 402 Ma with the predominant zircon peak of 350–360 Ma, consistent with the period of major magmatic activity of the Saur Arc (Chen et al., 2017b; Han et al., 2006; Luo et al., 2017; Yin et al., 2015; Yuan et al., 2007). These detrital zircon ages are different from those dating the magmatic activity of the Chingiz Arc, which was active from late Silurian to early Devonian times (Chen et al., 2010; Shen et al., 2012; Yin et al., 2017), and the 410–430 Ma peak is absent in the sediments in the Saur area. As a result, the source of the turbidites in the Saur area was more likely from the Saur Arc than the Chingiz Arc.

Regarding the detrital zircons in the turbidite (16-EM-147) situated at Hongguleleng in the Chingiz area, 47 spots yield detrital zircon ages ranging from 375 to 490 Ma except for one point of 603 Ma, which is consistent with that of previous work in the Chingiz area. For example, the greywacke (maybe part of the sequence; DJ-325) at Hongguleleng (Choulet, Cluzel, et al., 2012) contains detrital zircons with ages of 388–465 Ma with the main age peak at 424 ± 4 Ma and the youngest age at 388 ± 10 Ma. These ages are in agreement with the time of magma activity in the Chingiz Arc (Ren et al., 2014; Yang et al., 2015, 2017).

The Saur Arc formed by northward subduction, which was an opposite polarity to that of the Chingiz Arc (Chen et al., 2017a, 2017b). The Chingiz Arc formed in the period 410–430 Ma (Shen et al., 2012), whereas the Saur Arc was active only from 370 Ma (Shi et al., 2013; Wang et al., 2012) to the late Carboniferous. Clearly, the temporal and spatial evolution of the Saur and Chingiz arcs was completely different. Accordingly, the boundary of the two arcs is to the north of the Hebukesaier ophiolitic belt, marked in Figure 1b as the SCB.

7.5. Tectonic Model

The lithologies and geochronology of the Hebukesaier ophiolitic mélange provide the key information that indicates the evolution of the ocean crust from its generation to its demise. The structures and the provenance analysis of the sedimentary rocks in the ophiolitic mélange indicate that its northward accretion was caused by southward subduction, and information about the southward accretion of the Saur Arc (Chen et al., 2017a, 2017b) enables us to unravel the evolution and mutual boundary between the two arcs.

In the late Cambrian-middle Silurian, an ocean (its suture sited in the SCB; Han et al., 2010; He & Li, 2000, 2001) was one of the southern branches of the Palaeo-Asian Ocean. The age of the gabbro in the ophiolitic mélange (Zhao & He, 2014; Zhu & Xu, 2006) defines the formation time of the oceanic crust (Figure 12a).

In the middle Silurian to early Devonian (430–410 Ma), southward subduction beneath the active arc margin enabled dehydration of the subducted slab to generate the Chingiz Arc (Chen et al., 2010; Shen et al., 2012; Figure 12b).

From the early Devonian to late Carboniferous (410–306 Ma), southward subduction continued in the Chingiz area, when the conglomerates and breccias were accreted to the subduction complex, thereby recording the accretion process (Figure 12c).

From the late Carboniferous (306 Ma) to early late-Triassic (226 Ma), the ca. 262 Ma turbidite (Chen et al., 2017a) accreted to the accretionary prism in Saur area, indicating that accretion was continuous at this time. In the late Triassic (ca. 226 Ma), the diorite vein intruded into the accretionary complex, providing the

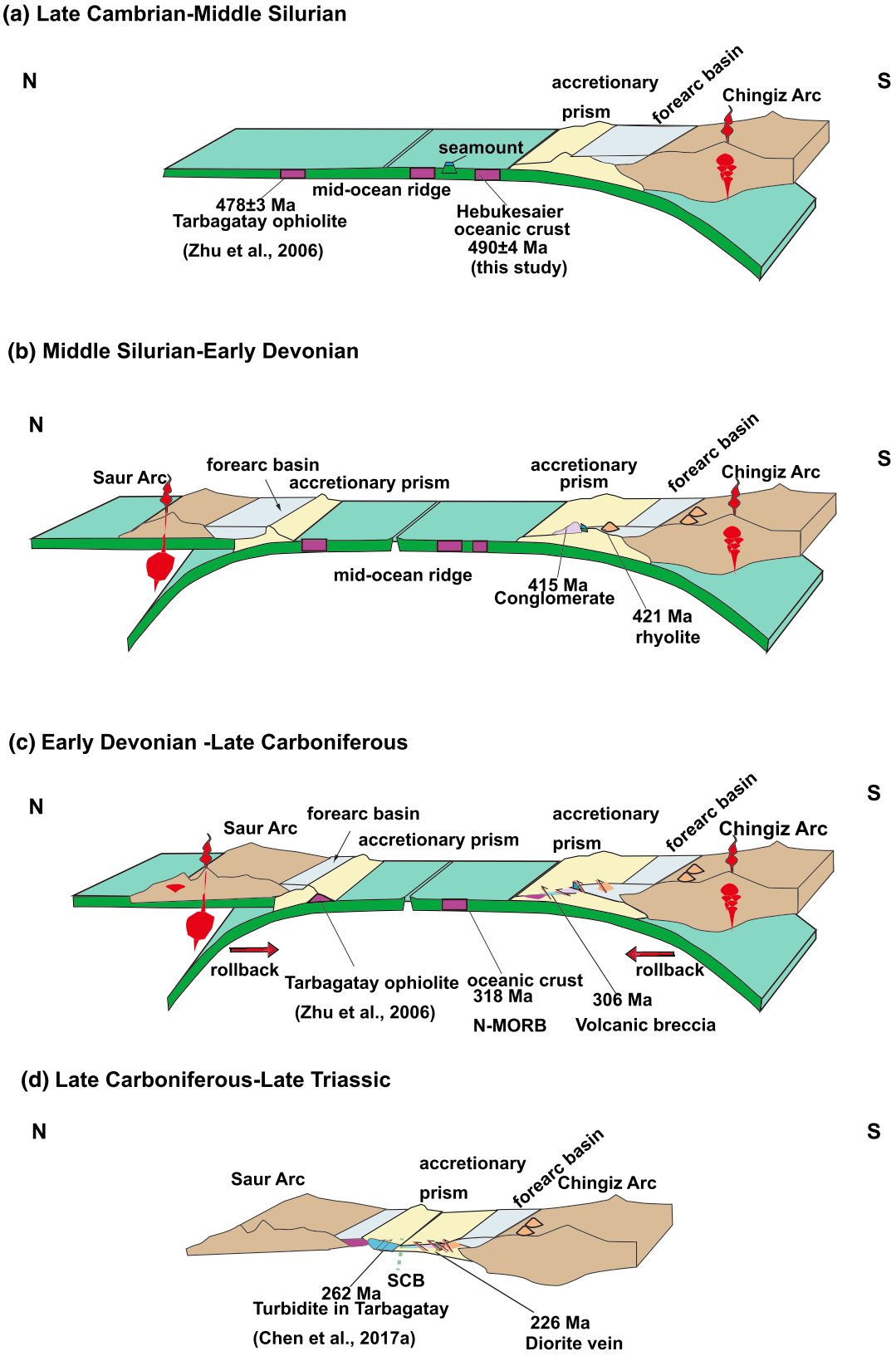

Figure 12. Time-diagrams portraying the evolution of accretionary complex in the Chingiz Arc and the Saur Arc in northwestern Junggar.

upper time limit of the closure of the ocean (Buslov et al., 2010; Tian et al., 2013, 2014; Xiao et al., 2018; Figure 12d).

8. CONCLUSIONS

Our new data and interpretations enable us to draw the following conclusions:

1. The Hebukesaier ophiolitic mélange in the SCB has a typical block-in-matrix structure. The gabbro and pillow basalts (Group I) exhibit N-MORB signatures, which indicate that the Hebukesaier ophiolite was generated in a mid-oceanic ridge setting. Zircon U-Pb ages of a coarse-grained gabbro, a fine-grained gabbro, and an intrusive diorite vein constrain the formation age of the ophiolitic mélange to be late Cambrian (ca. 490 Ma). The accretion of material from the subducting plate continued until the late Carboniferous (ca. 318 Ma). The diorite veins (ca. 226 Ma) provide an upper time limit for the termination of the subduction complex in the Chingiz area.
2. The kinematic data from the subduction complex indicate top-to-the-N thrusting and a southward polarity of subduction. The detrital zircon ages of the turbidites in the SCB indicate that the Chingiz Arc was the likely source area of the sediments in the Hebukesaier subduction complex. The detrital zircon ages and the structural kinematics independently suggest that subduction was to the south.
3. The Saur Arc was generated by northward subduction as in previous research, whereas the Chingiz Arc was by southward subduction. The tectonic boundary between the two arcs is located to the north of the Hebukesaier ophiolitic mélange within the SCB.

Data Availability Statement

The data in the manuscript are available in Mendeley Data repository (https://doi.org/10.17632/hzvfgrnx34.1).

Acknowledgments

Reimar Seltmann, Inna Sofanova, Min Sun, Guochun Zhao, and Baofu Han are thanked for useful discussions and suggestions. We appreciate editors and formal journal reviewers for their constructive comments. This study was financially supported by the National Key R & D Program of China (2017YFC0601206), the Strategic Priority Research Program (B) of the Chinese Academy of Sciences (XDB18020203), the National Natural Science Foundation of China (41730210, 41390441, 41472208, 41230207, and 41202150), and the Key Research Program of Frontier Sciences of CAS (QYZDJ-SSW-SYS012). We acknowledge the institutional support of PROGRESS Q45 (Charles University). This is a contribution to IGCP 662.

References

Abrajevitch, A., Van der Voo, R., Bazhenov, M. L., Levashova, N. M., & McCausland, P. J. (2008). The role of the Kazakhstan orocline in the late Paleozoic amalgamation of Eurasia. *Tectonophysics*, *455*(1-4), 61–76. https://doi.org/10.1016/j.tecto.2008.05.006

Abrajevitch, A., Van der Voo, R., Levashova, N. M., & Bazhenov, M. L. (2007). Paleomagnetic constraints on the paleogeography and oroclinal bending of the Devonian volcanic arc in Kazakhstan. *Tectonophysics*, *441*(1-4), 67–84. https://doi.org/10.1016/j.tecto.2007.04.008

Angiboust, S., Agard, P., De Hoog, J. C. M., Omrani, J., & Plunder, A. (2013). Insights on deep, accretionary subduction processes from the Sistan ophiolitic "mélange"(Eastern Iran). *Lithos*, *156*, 139–158. https://doi.org/10.1016/j.lithos.2012.11.007

Anonymous (1972). Penrose field conference on ophiolites. *Geotimes*, *17*(12), 24–25.

Buslov, M. M., Safonova, I. Y., Fedoseev, G. S., Reichow, M. K., Davies, K., & Babin, G. A. (2010). Permo-Triassic plume magmatism of the Kuznetsk Basin, Central Asia: Geology, geochronology, and geochemistry. *Russian Geology and Geophysics*, *51*(9), 1021–1036. https://doi.org/10.1016/j.rgg.2010.08.010

Cai, T. C. (1988). Ordovician and Silurian tetracorals from the southern part of Tarbagatai Mountain in Xinjiang. *Xinjiang Geology*, *2*, 007. (in Chinese with English abstract)

Cawood, P. A., Kröner, A., Collins, W. J., Kusky, T. M., Mooney, W. D., & Windley, B. F. (2009). Accretionary orogens through Earth history. *Geological Society of London, Special Publication*, *318*(1), 1–36. https://doi.org/10.1144/sp318.1

Chen, J. F., Han, B. F., Ji, J. Q., Zhang, L., Xu, Z., He, G. Q., & Wang, T. (2010). Zircon U-Pb ages and tectonic implications of Paleozoic plutons in northern West Junggar, North Xinjiang, China. *Lithos*, *115*(1-4), 137–152. https://doi.org/10.1016/j.lithos.2009.11.014

Chen, J. F., Han, B. F., Zhang, L., Xu, Z., Liu, J. L., Qu, W. J., et al. (2015). Middle Paleozoic initial amalgamation and crustal growth in the West Junggar (NW China): Constraints from geochronology, geochemistry and Sr–Nd–Hf–Os isotopes of calc-alkaline and alkaline intrusions in the Xiemisitai-Saier Mountains. *Journal of Asian Earth Sciences*, *113*, 90–109. https://doi.org/10.1016/j.jseaes.2014.11.028

Chen, Y. C., Xiao, W. J., Windley, B. F., Zhang, J. E., Sang, M., Li, R., et al. (2017a). Late Devonian-early Permian subduction-accretion of the Zharma-Saur oceanic arc, West Junggar (NW China): Insights from field geology, geochemistry and geochronology. *Journal of Asian Earth Sciences*, *145*, 424–445. https://doi.org/10.1016/j.jseaes.2017.06.010

Chen, Y. C., Xiao, W. J., Windley, B. F., Zhang, J. E., Zhou, K. F., & Sang, M. (2017b). Structures and detrital zircon ages of the Devonian–Permian Tarbagatay accretionary complex in west Junggar, China: Imbricated ocean plate stratigraphy and implications for amalgamation of the CAOB. *International Geology Review*, *59*(9), 1097–1115. https://doi.org/10.1080/00206814.2016.1185652

Choulet, F., Cluzel, D., Faure, M., Lin, W., Wang, B., Chen, Y., et al. (2012). New constraints on the pre-Permian continental crust growth of Central Asia (West Junggar, China) by U-Pb and Hf isotopic data from detrital zircon. *Terra Nova*, *24*(3), 189–198. https://doi.org/10.1111/j.1365-3121.2011.01052.x

Choulet, F., Faure, M., Cluzel, D., Chen, Y., Lin, W., & Wang, B. (2012). From oblique accretion to transpression in the evolution of the Altaid collage: New insights from West Junggar, northwestern China. *Gondwana Research*, *21*(2-3), 530–547. https://doi.org/10.1016/j.gr.2011.07.015

Choulet, F., Faure, M., Cluzel, D., Chen, Y., Lin, W., Wang, B., & Jahn, B. M. (2012). Architecture and evolution of accretionary orogens in the Altaids collage: The early Paleozoic West Junggar (NW China). *American Journal of Science*, *312*(10), 1098–1145. https://doi.org/10.2475/10.2012.02

Coleman, R. G. (1989). Continental growth of northwest China. *Tectonics*, *8*(3), 621–635. https://doi.org/10.1029/tc008i003p00621

Collins, A. S., & Robertson, A. H. F. (1997). Lycian melange, southwestern Turkey: An emplaced Late Cretaceous accretionary complex. *Geology*, *25*(3), 255–258. https://doi.org/10.1130/0091-7613(1997)025<0255:lmstae>2.3.co;2

Condie, K. C. (2007). Accretionary orogens in space and time. In R. D. Hatcher, Jr., M. P. Carlson, J. H. McBride, & J. R. Martínez Catalán (Eds.), *4-D framework of continental crust* (Vol. 200, pp. 145–158). Boulder, CO: Geological Society of America Memoirs.

Degtyarev, K. E., & Ryazantsev, A. V. (2007). Cambrian arc-continent collision in the Paleozoides of Kazakhstan. *Geotectonics*, *41*(1), 63–86. https://doi.org/10.1134/s0016852107010062

Du, H. Y., & Chen, J. F. (2017). The determination of Hoboksar Ancient Oceanic Basin in West Junngar: Evidence from zircon U-Pb age and geochemistry of the Hoboksar Ophiolitic mélange. *Acta Geologica Sinica*, *91*, 2638–2650. (in Chinese with English abstract)

Fu, D., Huang, B., Kusky, T. M., Li, G. Z., Wilde, S. A., Zhou, W. X., & Yu, Y. (2018). A middle Permian ophiolitic mélange belt in the Solonker suture zone, western Inner Mongolia, China: Implications for the evolution of the Paleo-Asian Ocean. *Tectonics*, *37*, 1292–1320. https://doi.org/10.1029/2017tc004947

Han, B. F., Guo, Z. J., Zhang, Z. C., Zhang, L., Chen, J. F., & Song, B. (2010). Age, geochemistry, and tectonic implications of a late Paleozoic stitching pluton in the North Tian Shan suture zone, western China. *GSA Bulletin*, *122*(3-4), 627–640. https://doi.org/10.1130/b26491.1

Han, B. F., Ji, J. Q., Song, B., Chen, L. H., & Zhang, L. (2006). Late Paleozoic vertical growth of continental crust around the Junggar Basin, Xinjiang, China (part I): Timing of post-collisional plutonism. *Acta Petrologica Sinica*, *22*(5), 1077–1086. (in Chinese with English abstract)

He, G. Q., & Li, M. S. (2000). New achievement in researching ophiolitic belts in central Asia and its significance in the links of tectonic belts between northern Xinjiang and adjacent area. *Xinjiang Geology*, *18*(3), 193–202. (in Chinese with English abstract)

He, G. Q., & Li, M. S. (2001). Significance of paleostructure and paleogeography of Ordovician-Silurian rock associations in northern Xinjiang, China. *Acta Scicentiarum Naturalum Universitis Pekinesis*, *37*(1), 99–110. (in Chinese with English abstract)

Hong, T., Klemd, R., Gao, J., Xiang, P., Xu, X. W., You, J., et al. (2017). The tectonic evolution of the Irtysh tectonic belt: New zircon U–Pb ages of arc-related and collisional granitoids in the Kalaxiangar tectonic belt NW China. *Lithos*, *272*, 46–68. https://doi.org/10.1016/j.lithos.2016.12.001

Kröner, A., Windley, B. F., Badarch, G., Tomurtogoo, O., Hegner, E., Jahn, B. M., et al. (2007). Accretionary growth and crust formation in the Central Asian Orogenic Belt and comparison with the Arabian-Nubian shield. *Memoir-Geological Society of America*, *200*, 181. https://doi.org/10.1130/2007.1200(11)

Kusky, T. M., Bradley, D. C., Haeussler, P. J., & Karl, S. (1997). Controls on accretion of flysch and mélange belts at convergent margins: Evidence from the Chugach Bay thrust and Iceworm mélange, Chugach accretionary wedge, Alaska. *Tectonics*, *16*(6), 855–878. https://doi.org/10.1029/97tc02780

Kusky, T. M., Windley, B. F., Safonova, I., Wakita, K., Wakabayashi, J., Polat, A., & Santosh, M. (2013). Recognition of ocean plate stratigraphy in accretionary orogens through Earth history: A record of 3.8 billion years of sea floor spreading, subduction, and accretion. *Gondwana Research*, *24*(2), 501–547. https://doi.org/10.1016/j.gr.2013.01.004

Li, P. F., Sun, M., Rosenbaum, G., Jourdan, F., Li, S. Z., & Cai, K. D. (2017). Late Paleozoic closure of the Ob-Zaisan Ocean along the Irtysh shear zone (NW China): Implications for arc amalgamation and oroclinal bending in the Central Asian orogenic belt. *GSA Bulletin*, *129*(5-6), 547–569. https://doi.org/10.1130/b31541.1

Li, P. F., Sun, M., Rosenbaum, G., Yuan, C., Safonova, I., Cai, K., et al. (2018). Geometry, kinematics and tectonic models of the Kazakhstan Orocline Central Asian Orogenic Belt. *Journal of Asian Earth Sciences*, *153*, 42–56. https://doi.org/10.1016/j.jseaes.2017.07.029

Li, T. D., & Poliyangsiji, B. H. (2001). Tectonics and crustal evolution of Altay in China and Kazakhstan. *Xinjiang Geology*, *19*, 27–32. (in Chinese)

Liu, X. M., Chen, Y. L., Li, D. P., Wang, Z., & Liu, J. B. (2010). The U-Pb ages and Hf isotopes of zircons in the metadiabase and gneissic granite, Beishan orogenic belt, Inner Mongolia, China and its significance. *Geological Bulletin of China*, *29*(4), 518–529. (in Chinese with English abstract)

Liu, Y. S., Hu, Z. C., Gao, S., Günther, D., Xu, J., Gao, C. G., & Chen, H. H. (2008). In situ analysis of major and trace elements of anhydrous minerals by LA-ICP-MS without applying an internal standard. *Chemical Geology*, *257*(1-2), 34–43. https://doi.org/10.1016/j.chemgeo.2008.08.004

Ludwig, K. R. (2003). User's manual for IsoPlot 3.0. In *A geochronological toolkit for Microsoft Excel* (Vol. 71, pp. 1–74. Berkeley, CA: Berkeley Geochronology Center.

Luo, J., Xiao, W. J., Wakabayashi, J., Han, C. M., Zhang, J. E., Wan, B., et al. (2017). The Zhaheba ophiolite complex in Eastern Junggar (NW China): Long lived supra-subduction zone ocean crust formation and its implications for the tectonic evolution in southern Altaids. *Gondwana Research*, *43*, 17–40. https://doi.org/10.1016/j.gr.2015.04.004

Meng, L., Shen, P., Shen, Y. C., Liu, T. B., Song, G. X., Dai, H. W., et al. (2010). Igneous rocks geochemistry, zircon U-Pb age and its geological significance in the central section of Xiemisitai area, Xinjiang. *Acta Petrologica Sinica*, *26*(10), 3047–3056. (in Chinese with English abstract)

Mutti, E., & Normark, W. R. (1987). Comparing examples of modern and ancient turbidite systems: Problems and concepts. In *Marine clastic sedimentology* (pp. 1–38). London, UK: Springer.

Mutti, E., Tinterri, R., Benevelli, G., di Biase, D., & Cavanna, G. (2003). Deltaic, mixed and turbidite sedimentation of ancient foreland basins. *Marine and Petroleum Geology*, *20*(6-8), 733–755. https://doi.org/10.1016/j.marpetgeo.2003.09.001

Passchier, C. W., & Trouw, R. A. J. (2005). *Microtectonics*. Berlin, Germany: Springer Science & Business Media.

Pearce, J. A. (2008). Geochemical fingerprinting of oceanic basalts with applications to ophiolite classification and the search for Archean oceanic crust. *Lithos*, *100*(1-4), 14–48. https://doi.org/10.1016/j.lithos.2007.06.016

Pearce, J. A. (2014). Immobile element fingerprinting of ophiolites. *Elements*, *10*(2), 101–108. https://doi.org/10.2113/gselements.10.2.101

Pearce, J. A., & Cann, J. R. (1973). Tectonic setting of basic volcanic rocks determined using trace element analyses. *Earth and Planetary Science Letters*, *19*(2), 290–300. https://doi.org/10.1016/0012-821x(73)90129-5

Pearce, J. A., & Peate, D. W. (1995). Tectonic implications of the composition of volcanic arc magmas. *Annual Review of Earth and Planetary Sciences*, *23*(1), 251–285. https://doi.org/10.1146/annurev.ea.23.050195.001343

Pearce, N. J. G., Perkins, W. T., Westgate, J. A., Gorton, M. P., Jackson, S. E., Neal, C. R., & Chenery, S. P. (1997). A compilation of new and published major and trace element data for NIST SRM 610 and NIST SRM 612 glass reference materials. *Geostandards and Geoanalytical Research*, *21*(1), 115–144. https://doi.org/10.1111/j.1751-908x.1997.tb00538.x

Ren, R., Han, B. F., Xu, Z., Zhou, Y. Z., Liu, B., Zhang, L., et al. (2014). When did the subduction first initiate in the southern Paleo-Asian Ocean: New constraints from a Cambrian intra-oceanic arc system in West Junggar NW China. *Earth and Planetary Science Letters*, *388*, 222–236. https://doi.org/10.1016/j.epsl.2013.11.055

Safonova, I., Biske, G., Romer, R. L., Seltmann, R., Simonov, V., & Maruyama, S. (2016). Middle Paleozoic mafic magmatism and ocean plate stratigraphy of the South Tianshan, Kyrgyzstan. *Gondwana Research*, *30*, 236–256. https://doi.org/10.1016/j.gr.2015.03.006

Safonova, I., Komiya, T., Romer, R. L., Simonov, V., Seltmann, R., Rudnev, S., et al. (2018). Supra-subduction igneous formations of the Char ophiolite belt East Kazakhstan. *Gondwana Research*, *59*, 159–179. https://doi.org/10.1016/j.gr.2018.04.001

Safonova, I., Kotlyarov, A., Krivonogov, S., & Xiao, W. J. (2017). Intra-oceanic arcs of the Paleo-Asian Ocean. *Gondwana Research*, *50*, 167–194. https://doi.org/10.1016/j.gr.2017.04.005

Şengör, A. M. C., & Natal'In, B. A. (1996). Turkic-type orogeny and its role in the making of the continental crust. *Annual Review of Earth and Planetary Sciences*, *24*(1), 263–337. https://doi.org/10.1146/annurev.earth.24.1.263

Şengör, A. M. C., Natal'in, B. A., & Burtman, V. S. (1993). Evolution of the Altaid tectonic collage and Palaeozoic crustal growth in Eurasia. *Nature*, *364*(6435), 299–307. https://doi.org/10.1038/364299a0

Şengör, A. M. C., Natal'in, B. A., Sunal, G., & van der Voo, R. (2018). The tectonics of the Altaids: Crustal growth during the construction of the continental lithosphere of Central Asia between≁ 750 and≁ 130 Ma ago. *Annual Review of Earth and Planetary Sciences*, *46*, 439–494. https://doi.org/10.1146/annurev-earth-060313-054826

Shen, P., Pan, H. D., Seitmuratova, E., Yuan, F., & Jakupova, S. (2015). A Cambrian intra-oceanic subduction system in the Bozshakol area Kazakhstan. *Lithos*, *224*, 61–77. https://doi.org/10.1016/j.lithos.2015.02.025

Shen, P., Pan, H. D., Shen, Y. C., Yan, Y. H., & Zhong, S. H. (2015). Main deposit styles and associated tectonics of the West Junggar region, NW China. *Geoscience Frontiers*, *6*(2), 175–190. https://doi.org/10.1016/j.gsf.2014.05.001

Shen, P., Shen, Y. C., Li, X. H., Pan, H. D., Zhu, H. P., Meng, L., & Dai, H. W. (2012). Northwestern Junggar Basin, Xiemisitai Mountains, China: A geochemical and geochronological approach. *Lithos*, *140*, 103–118. https://doi.org/10.1016/j.lithos.2012.02.004

Shi, Y., Wang, Y. W., Wang, J. B., Wang, L. J., Ding, R. F., & Chen, Y. F. (2013). Zircon U-Pb age, geochemistry and geological implications of granitoids in Tuerkubantao, Xinjiang. *Journal of Earth Science*, *24*(4), 606–618. https://doi.org/10.1007/s12583-013-0360-z

Sugiyama, K. (1977). Triassic and Lower Jurassic radiolarian biostratigraphy in the siliceous claystone and bedded chert units of the southeastern Mino Terrane Central Japan. *Bulletin of Mizunami Fossil Museum*, *24*, 79–193.

Sun, S. S., & McDonough, W. F. S. (1989). Chemical and isotopic systematics of oceanic basalts: Implications for mantle composition and processes. *Geological Society of London, Special Publication*, *42*(1), 313–345. https://doi.org/10.1144/gsl.sp.1989.042.01.19

Tian, Z. H., Xiao, W. J., Shan, Y. H., Windley, B. F., Han, C. M., Zhang, J. E., & Song, D. F. (2013). Mega-fold interference patterns in the Beishan orogen (NW China) created by change in plate configuration during Permo-Triassic termination of the Altaids. *Journal of Structural Geology*, *52*, 119–135. https://doi.org/10.1016/j.jsg.2013.03.016

Tian, Z. H., Xiao, W. J., Windley, B. F., Lin, L. N., Han, C. M., Zhang, J. E., et al. (2014). Structure, age, and tectonic development of the Huoshishan–Niujuanzi ophiolitic mélange, Beishan, southernmost Altaids. *Gondwana Research*, *25*(2), 820–841. https://doi.org/10.1016/j.gr.2013.05.006

Wakabayashi, J. (2012). Subducted sedimentary serpentinite mélanges: Record of multiple burial–exhumation cycles and subduction erosion. *Tectonophysics*, *568*, 230–247. https://doi.org/10.1016/j.tecto.2011.11.006

Wakita, K. (2015). OPS mélange: A new term for mélanges of convergent margins of the world. *International Geology Review*, *57*(5-8), 529–539. https://doi.org/10.1080/00206814.2014.949312

Wakita, K., & Metcalfe, I. (2005). Ocean plate stratigraphy in East and Southeast Asia. *Journal of Asian Earth Sciences*, *24*(6), 679–702. https://doi.org/10.1016/j.jseaes.2004.04.004

Wakita, K., Pubellier, M., & Windley, B. F. (2013). Tectonic processes, from rifting to collision via subduction, in SE Asia and the western Pacific: A key to understanding the architecture of the Central Asian Orogenic Belt. *Lithosphere*, *5*(3), 265–276. https://doi.org/10.1130/l234.1

Wan, B., Windley, B. F., Xiao, W. J., Feng, J. Y., & Zhang, J. E. (2015). Paleoproterozoic high-pressure metamorphism in the northern North China Craton and implications for the Nuna supercontinent. *Nature Communications*, *6*(1), 8344. https://doi.org/10.1038/ncomms9344

Wang, B., Faure, M., Cluzel, D., Shu, L. S., Charvet, J., Meffre, S., & Ma, Q. (2006). Late Paleozoic tectonic evolution of the northern West Chinese Tianshan belt. *Geodinamica Acta*, *19*(3-4), 237–247. https://doi.org/10.3166/ga.19.237-247

Wang, M., Zhang, J. J., Pei, X. Z., Liu, K., Zhang, B., & Chen, Y. X. (2018). Significant Carboniferous magmatism and continental growth in the northern West Tianshan orogen NW China: Revealed by detrital zircon U-Pb and Lu-Hf analyses for turbidites from the North Tianshan Accretionary Complex. *Journal of Geodynamics*, *118*, 11–31. https://doi.org/10.1016/j.jog.2018.04.006

Wang, Y. W., Wang, J. B., Wang, L. J., Long, L. L., Tang, P. Z., Liao, Z., et al. (2012). The Tuerkubantao ophiolite mélange in Xinjiang, NW China: New evidence for the Erqis suture zone. *Geoscience Frontiers*, *3*(5), 587–602. https://doi.org/10.1016/j.gsf.2012.02.002

Wang, Z. Q., Jiang, X. M., Guo, J., Xu, F., Deng, X., Zhang, Q., et al. (2014). Discovery of the Early Paleozoic Volcanic Rocks in the Xiemisitai Area of the Western Junggar, Xinjiang. *Geotectonica et Metallogenia*, *38*(3), 670–685. (in Chinese with English abstract)

Wilhem, C., Windley, B. F., & Stampfli, G. M. (2012). The Altaids of Central Asia: A tectonic and evolutionary innovative review. *Earth-Science Reviews*, *113*(3-4), 303–341. https://doi.org/10.1016/j.earscirev.2012.04.001

Windley, B. F., Alexeiev, D., Xiao, W. J., Kroner, A., & Badarch, G. (2007). Tectonic models for accretion of the Central Asian Orogenic Belt. *Journal of the Geological Society*, *164*(1), 31–47. https://doi.org/10.1144/0016-76492006-022

Windley, B. F., & Xiao, W. J. (2018). Ridge subduction and slab windows in the Central Asian Orogenic Belt: Tectonic implications for the evolution of an accretionary orogen. *Gondwana Research*, *61*, 73–87. https://doi.org/10.1016/j.gr.2018.05.003

Wood, D. A. (1980). The application of a Th-Hf-Ta diagram to problems of tectonomagmatic classification and to establishing the nature of crustal contamination of basaltic lavas of the British Tertiary Volcanic Province. *Earth and Planetary Science Letters*, *50*(1), 11–30. https://doi.org/10.1016/0012-821x(80)90116-8

Workman, R. K., & Hart, S. R. (2005). Major and trace element composition of the depleted MORB mantle (DMM). *Earth and Planetary Science Letters*, *231*(1), 53–72. https://doi.org/10.1016/j.epsl.2004.12.005

Xiang, K. P., Li, Y. J., Yang, Y., Wang, R., Yang, G. X., Sun, Y., & Wang, J. N. (2015). LA ICP-MS zircon age, geochemistry and tectonic setting of the volcanic rocks from the Late Devonian Tieliketi Formation in the Ur Kashgar Mountain, western Junggar. *Acta Petrologica Sinica*, *31*(2), 534–544. (in Chinese with English abstract)

Xiao, W. J., Ao, S. J., Yang, L., Han, C. M., Wan, B., Zhang, J. E., et al. (2017). Anatomy of composition and nature of plate convergence: Insights for alternative thoughts for terminal India-Eurasia collision. *Science China Earth Sciences*, *60*(6), 1015–1039. https://doi.org/10.1007/s11430-016-9043-3

Xiao, W. J., Han, C. M., Liu, W., Wan, B., Zhang, J. E., Ao, S. J., et al. (2014). How many sutures in the southern Central Asian Orogenic Belt: Insights from East Xinjiang–West Gansu (NW China)? *Geoscience Frontiers*, *5*(4), 525–536. https://doi.org/10.1016/j.gsf.2014.04.002

Xiao, W. J., Huang, B. C., Han, C. M., Sun, S., & Li, J. L. (2010). A review of the western part of the Altaids: A key to understanding the architecture of accretionary orogens. *Gondwana Research*, *18*(2-3), 253–273. https://doi.org/10.1016/j.gr.2010.01.007

Xiao, W. J., Windley, B. F., Han, C. M., Liu, W., Wan, B., Zhang, J. E., et al. (2018). Late Paleozoic to early Triassic multiple roll-back and oroclinal bending of the Mongolia collage in Central Asia. *Earth-Science Reviews*, *186*, 94–128. https://doi.org/10.1016/j.earscirev.2017.09.020

Xiao, W. J., Windley, B. F., Hao, J., & Zhai, M. G. (2003). Accretion leading to collision and the Permian Solonker suture, Inner Mongolia, China: Termination of the central Asian orogenic belt. *Tectonics*, *22*(6), 1069. https://doi.org/10.1029/2002tc001484

Xiao, W. J., Windley, B. F., Sun, S., Li, J. L., Huang, B. C., Han, C. M., et al. (2015). A tale of amalgamation of three Permo-Triassic collage systems in Central Asia: Oroclines, sutures, and terminal accretion. *Annual Review of Earth and Planetary Sciences*, *43*(1), 477–507. https://doi.org/10.1146/annurev-earth-060614-105254

Yang, G. X., Li, Y. J., Tong, L. L., Wang, Z. P., & Xu, Q. (2017). Petrogenesis of pillow basalts in West Junggar, NW China: Constraints from geochronology, geochemistry, and Sr–Nd–Pb isotopes. *Geological Journal*, *54*(4), 1815–1833. https://doi.org/10.1002/gj.3078

Yang, G. X., Li, Y. J., Xiao, W. J., & Tong, L. L. (2015). OIB-type rocks within West Junggar ophiolitic mélanges: Evidence for the accretion of seamounts. *Earth-Science Reviews*, *150*, 477–496. https://doi.org/10.1016/j.earscirev.2015.09.002

Yang, Y. Q., Zhao, L., Xu, Q., Zheng, R. G., & Niu, B. G. (2018). Determination of the Hebukesaier Ophiolitic Melange in the Northern Part of West Junggar and its Tectonic Implications. *Acta Geologica Sinica*, *92*, 298–312. (in Chinese with English abstract)

Yin, J. Y., Chen, W., Xiao, W. J., Yuan, C., Sun, M., & Cai, K. D. (2018). Petrogenesis and tectonic implications of early Devonian mafic dike–granite association in the northern West Junggar, NW China. *International Geology Review*, *60*(1), 87–100. https://doi.org/10.1080/00206814.2017.1323238

Yin, J. Y., Chen, W., Xiao, W. J., Yuan, C., Windley, B. F., Yu, S., & Cai, K. D. (2017). Late Silurian–early Devonian adakitic granodiorite A-type and I-type granites in NW Junggar, NW China: Partial melting of mafic lower crust and implications for slab roll-back. *Gondwana Research*, *43*, 55–73. https://doi.org/10.1016/j.gr.2015.06.016

Yin, J. Y., Chen, W., Yuan, C., Yu, S., Xiao, W. J., Long, X. P., et al. (2015). Petrogenesis of Early Carboniferous adakitic dikes, Sawur region, northern West Junggar, NW China: Implications for geodynamic evolution. *Gondwana Research*, *27*(4), 1630–1645. https://doi.org/10.1016/j.gr.2014.01.016

Yuan, C., Sun, M., Xiao, W., Li, X., Lin, S., Zhang, J., et al. (2006). Paleozoic accretion of Chinese Altai: Geochronological constraints from granitoids. *Abstract of Western Pacific Geophysics Meeting, CD-ROM*. Beijing, China.

Yuan, C., Sun, M., Xiao, W. J., Li, X. H., Chen, H. L., Lin, S. F., et al. (2007). Accretionary orogenesis of the Chinese Altai: Insights from Paleozoic granitoids. *Chemical Geology*, *242*(1-2), 22–39. https://doi.org/10.1016/j.chemgeo.2007.02.013

Zhang, D. Y., Zhou, T. F., & Yuan, F. (2015). The discovery on the Early Paleozoic magmatism in the Sawuer area, West Jungaar. *Acta Petrologica Sinica*, *31*(2), 415–425. (in Chinese with English abstract)

Zhang, J. E., Xiao, W. J., Han, C. M., Ao, S. J., Yuan, C., Sun, M., et al. (2011). Kinematics and age constraints of deformation in a Late Carboniferous accretionary complex in Western Junggar, NW China. *Gondwana Research*, *19*(4), 958–974. https://doi.org/10.1016/j.gr.2010.10.003

Zhang, J. E., Xiao, W. J., Han, C. M., Mao, Q. G., Ao, S. J., Guo, Q. Q., & Ma, C. (2011). A Devonian to Carboniferous intra-oceanic subduction system in Western Junggar, NW China. *Lithos*, *125*(1-2), 592–606. https://doi.org/10.1016/j.lithos.2011.03.013

Zhang, J. E., Xiao, W. J., Luo, J., Chen, Y. C., Windley, B. F., Song, D. F., et al. (2018). Collision of the Tacheng block with the Mayile-Barleik-Tangbale accretionary complex in Western Junggar NW China: Implication for Early-Middle Paleozoic architecture of the western Altaids. *Journal of Asian Earth Sciences*, *159*, 259–278. https://doi.org/10.1016/j.jseaes.2017.03.023

Zhang, Y. Y., & Guo, Z. J. (2010). New constraints on formation ages of ophiolites in northern Junggar and comparative study on their connection. *Acta Petrologica Sinica*, *26*(2), 421–430. (in Chinese with English abstract)

Zhao, L., & He, G. Q. (2014). Geochronology and geochemistry of the Cambrian (~518 Ma) Chagantaolegai ophiolite in northern West Junggar (NW China): constraints on spatiotemporal characteristics of the Chingiz–Tarbagatai megazone. *International Geology Review*, *56*(10), 1181–1196. https://doi.org/10.1080/00206814.2014.926783

Zhou, T. F., Yuan, F., Fan, Y., Zhang, D. Y., Cooke, D., & Zhao, G. C. (2008). Granites in the Sawuer region of the west Junggar, Xinjiang Province, China: geochronological and geochemical characteristics and their geodynamic significance. *Lithos*, *106*(3-4), 191–206. https://doi.org/10.1016/j.lithos.2008.06.014

Zhu, Y. F., & Xu, X. (2006). The discovery of Early Ordovician ophiolite melange in Taerbahatai Mts Xinjiang, NW China. *Acta Petrologica Sinica*, *22*(12), 2833–2842. (in Chinese with English abstract)

Zong, K. Q., Klemd, R., Yuan, Y., He, Z. Y., Guo, J. L., Shi, X. L., et al. (2017). The assembly of Rodinia: The correlation of early Neoproterozoic (ca. 900 Ma) high-grade metamorphism and continental arc formation in the southern Beishan Orogen, southern Central Asian Orogenic Belt (CAOB). *Precambrian Research*, *290*, 32–48. https://doi.org/10.1016/j.precamres.2016.12.010